

Gamma and Theta Rhythms in Biophysical Models of Hippocampal Circuits

N. Kopell, C. Börgers, D. Pervouchine, P. Malerba, and A. Tort

Introduction

The neural circuits of the hippocampus are extremely complex, with many classes of interneurons whose contributions to network dynamics and function are still unknown. Nevertheless, reduced models can provide insight into aspects of the dynamics and associated function. In this chapter, we discuss models at a variety of levels of complexity, all simple enough to probe the reasons for the behavior of the model. The chapter focuses on the main rhythms displayed by the hippocampus, the gamma (30–90 Hz) and theta (4–12 Hz) rhythms. We concentrate on modeling *in vitro* experiments, but with an eye toward possible *in vivo* implications.

Models of gamma and theta rhythms range from very detailed, biophysically realistic descriptions to abstract caricatures. At the most detailed levels, the cells are described by Hodgkin–Huxley-type equations, with many different cell types and large numbers of ionic currents and compartments (Traub et al., 2004). We use simpler biophysical models; all cells have a single compartment only, and the interneurons are restricted to two types: fast-spiking (FS) basket cells and oriens lacunosum-moleculare (O-LM) cells. Unlike Traub et al. (2004), we aim not so much at reproducing dynamics in great detail, but at clarifying the essential mechanisms underlying the production of the rhythms and their interactions (Kopell, 2005). In particular, we wish to highlight the dynamical as well as physiological mechanisms associated with rhythms, and to begin to classify them by mechanisms, not just frequencies.

One theme in this chapter is the interaction of gamma and theta rhythms. To understand this interaction, it is necessary to describe the mechanisms of the gamma and theta rhythms separately before putting them together. A second theme is the use of mathematical tools to get a deeper understanding of the dynamics of rhythmic networks. We apply these ideas mainly to the question of how networks can produce

N. Kopell (✉)

Department of Mathematics and Center for BioDynamics, Boston University, Boston, MA 02215, USA

e-mail: nk@math.bu.edu

a theta rhythm from cells that do not naturally synchronize. A final theme is the use of model networks to understand how dynamics contributes to function.

To maintain coherence, we use the same models for our interneurons and pyramidal cells in all sections of the chapter. Similarly, we use the same models for synapses in each section. These models are closely related, but not identical, to other models previously published (Acker et al., 2003; Pervouchine et al., 2006; Gloveli et al., 2005b; Börgers et al., 2005; Börgers and Kopell, 2003, 2005, 2008). Different versions of the same rhythms are produced by the same general model, but with different parameter sets. All the equations and parameters employed throughout this chapter are given in the appendices. Several different codes were used to generate the simulation results in this chapter; all codes, with manuals for their use, are included on the disk.

Gamma Rhythms, in Various Guises

The circumstances under which the gamma rhythm is observed both in vivo and in vitro are described in chapter “Neuronal Activity Patterns During Hippocampal Network Oscillation In Vitro” (see also Whittington et al., 2000). As we will discuss below, we believe that the gamma rhythm is important for the creation, modulation, and protection of cell assemblies. How that happens depends on the mechanisms associated with the formation of this rhythm, and so we focus below on these mechanisms.

The name “gamma rhythm” has been used to denote rhythms in a very large range of frequencies, from 20 Hz to over 100 Hz. We use here a more limited definition: we define the gamma rhythm to be neural dynamics in which the population of basket cells (and/or other FS interneurons) fires rhythmically on a time scale dependent on the decay time of inhibitory postsynaptic potentials (Whittington et al., 2000). In practice, that restricts the gamma range to approximately 30–90 Hz. The high-frequency rhythms seen in neocortex (Canolty et al., 2006) and hippocampus and striatum (Tort et al., 2008) are not considered gamma in this mechanistically based nomenclature.

The gamma rhythm is found in many structures of the brain, including the cerebral cortex and the entorhinal cortex (EC). Though there are some differences between gamma rhythms in different parts of the brain (Cunningham et al., 2004), the models we discuss do not make use of specific properties of hippocampal neurons. The gamma rhythm is treated in the models discussed below as an interaction of pyramidal cells and FS cells (or sometimes just as an interaction among FS cells). We treat both the FS cells and the pyramidal cells as single compartments with minimal currents: the spiking Na^+ and K^+ currents, leak, and the synaptic GABA_A and AMPA currents. The gamma rhythms discussed here are believed to be formed near the somata of the pyramidal cells (Buhl et al., 1995), justifying a one-compartment model of those cells.

An essential feature of the gamma models discussed here is that the decay time of the GABA_A current is the longest time scale in the system; in particular, it is longer

than the membrane time “constant” of either of the cell types involved. The latter hypothesis seems counter-factual at first: the membrane time constant is often taken to be about 10 ms or more (see Whittington et al., 1996), while the unitary IPSC decay time constant has been measured in some contexts to be less than 2 ms (Bartos et al., 2001, 2002). The central point is that the above measurements were not taken in the context of ongoing gamma oscillations, in which the decay time has been measured to be about 8–12 ms. It is not known if the unitary IPSCs are longer in the context of an oscillating network. It may also be that other interneurons play a role in the gamma oscillations, and that they have longer IPSCs. Finally, when the network is producing a gamma rhythm, the basket cell interneurons are highly correlated, but may not be exactly synchronous, and hence produce population IPSCs that take longer to decay. Since there are far fewer cells in the model networks than in real brain networks, each model synapse represents a large number of real synapses. For these reasons, we have chosen to use parameters derived directly from the gamma oscillations rather than the technically more accurate measurements (Bartos et al., 2001, 2002) from situations that are less relevant to the data we model.

The issue of the membrane time is more subtle. This “constant” actually changes dynamically, along with the currents expressed at any moment: the larger the sum of the intrinsic and synaptic currents, the smaller the instantaneous membrane time. With an inhibitory decay time in the above range, and the maximal inhibitory conductance an order of magnitude larger than the resting conductance (Whittington et al., 1996), the effective membrane time is small for at least half the gamma cycle. With instantaneous membrane times short enough for a long enough period, voltages “equilibrate” to the instantaneous inhibitory current, rendering the neurons’ history irrelevant for their future behavior. This was spelled out in Börgers and Kopell (2005) for a reduced model, and we find the same behavior in our physiological models. The lack of history dependence turns out to be central for some of the functional implications of the gamma rhythms (e.g. see section “PING and Cell Assemblies”). The exact choice of the membrane time is not critical, provided it is not too long relative to the inhibitory decay time. In the work by Bartos et al. on models of gamma oscillations in networks of GABAergic interneurons, the inhibitory time constant is very short, but the maximal inhibitory conductance is chosen to be two orders of magnitude larger than the resting conductance; this is quite different from our parameter regime and may lead to different conclusions.

Real pyramidal cells have a multitude of other currents (Traub et al., 2005). However, we hypothesize that the other currents are not important for some kinds of gamma rhythms (see PING below); for other kinds, they modulate the properties, but are not critical for the existence of the rhythms. Some of the other currents, such as the hyperpolarization-activated h-current, are inactive at the high voltage ranges associated with gamma. During spiking, others may be swamped by the size of the spiking currents. The high frequency of the gamma rhythm may not allow currents with slow kinetics to change much during the interspike interval. Thus, though the kinetics of pyramidal cells can be very complex, especially in the dendritic integration, the aspects that are important to the gamma rhythm can be captured in models as simple as integrate-and-fire.

The rhythms that occur in the gamma frequency range are not all the same mechanistically, either in vivo or in vitro. In vitro, rhythms in the 30–50 Hz range can be produced in the hippocampus in at least three qualitatively different ways: Interneuronal network gamma (ING), pyramidal-interneuronal network gamma (PING), and persistent gamma (see chapter “Neuronal Activity Patterns During Hippocampal Network Oscillation In Vitro” for details). These are distinguished less by their different frequencies than by the sets of neurons that are involved. In ING, the effects of the AMPA synapses are blocked, so that only inhibitory cells are involved, and these fire at or near the population frequency. In PING, both excitatory and inhibitory cells are involved, with both classes of cells firing at or near the population frequency. In vitro PING is a short-lived phenomenon induced by tetanic stimulation. Persistent gamma, produced pharmacologically, lasts for hours; in this version of the gamma rhythm, FS cells fire at close to population frequency, while the pyramidal cells fire at much lower rates (see chapter “Neuronal Activity Patterns During Hippocampal Network Oscillation In Vitro”). In all three of these forms of gamma, the population frequency depends on the decay time of GABA_A-receptor mediated synapses. Since the ING rhythm plays no role in our discussion of the interaction of gamma and theta rhythms, we will not say much more about it; see Kopell and Ermentrout (2004) for references. The code for simulating gamma rhythms that we include with this chapter is capable of producing all three kinds of gamma. We give the parameter values associated with PING and persistent gamma in Appendix 2.

PING

The PING rhythm has been modeled in a variety of ways, from the very detailed (Traub et al., 1997) to the very simple (Ermentrout and Kopell, 1998). In discussing model pyramidal and FS cells, we will use the abbreviations E- and I-cells (for excitatory and inhibitory). A cycle of the PING rhythm begins with a surge in spiking of the E-cells, which triggers a surge in spiking of the I-cells. The resulting pulse of inhibitory input to the E-cells brings them closer to synchrony. When inhibition wears off, the E-cells resume spiking, and the cycle repeats. The period of the rhythm depends primarily on the decay time constant of the GABA_A synapses, less on the strengths of those synapses and the excitability of the E-cells (Börgers and Kopell, 2005, Eq. (3.15)). A key step in the analysis of the PING mechanism is to explain why and when a common inhibitory input pulse has a synchronizing effect on a population of neurons. The effect of the inhibition is to create, transiently, a stable fixed point. All trajectories move toward this fixed point, thereby getting close to each other. The synchronization can be interpreted as the effect of an attracting river (Diener, 1985a,b) in a phase space that includes the decaying strength of inhibition as a dependent variable (Börgers and Kopell, 2005).

Assuming E-cells of type I (Ermentrout, 1996), the PING mechanism works if the following conditions hold (Börgers and Kopell, 2003):

- (1) The E-cells receive external input that would drive them, in the absence of any synaptic input, at or above gamma frequency.

- (2) The E→I synapses are so strong and have so short a rise time that a surge in spiking of the E-cells quickly triggers a surge in spiking of the I-cells.
- (3) The I-cells spike only in response to the E-cells.
- (4) The I→E synapses are strong enough that a population spike of the I-cells approximately synchronizes the E-cells.

The analysis of the PING mechanism becomes more complicated if there is noise and/or heterogeneity in the network. It has been shown (Golomb and Hansel, 2000; Börgers and Kopell, 2003) that the formation of a coherent gamma rhythm depends on the number of connections to a given E- or I-cell from the opposite population, independent of the size of the network; thus, the connections can be arbitrarily sparse. The analysis of Börgers and Kopell (2003) shows that the I-cells are typically synchronized more tightly than the E-cells. Further analysis also shows that, while ING is vulnerable to heterogeneity (Wang and Buzsáki, 1996; White et al., 1998a), PING is more robust. (ING becomes robust if gap junctions are added to the network; see Kopell and Ermentrout, 2004 and Traub et al., 2001). However, PING can be destroyed by too much noise, especially when the excitability of the E- and I-cells is low, and so the frequency of the network is also low. For frequencies above of about 90 Hz, the rhythm is often quite sensitive to heterogeneity. Hence the PING mechanism operates best in the 30–90 Hz regime (Börgers and Kopell, 2005).

The analysis of PING rhythms enables one to understand how modulation of the network, which changes network parameters, can lead to loss of rhythmicity. In particular, the PING mechanism breaks down when the drive to the I-cells becomes too large relative to the drive to the E-cells. In a simple 2-cell network, the I-cell fires without being prompted by the E-cell, leading to “phase walk-through.” In larger networks of E- and I-cells, the rhythmicity is typically lost in a different manner: the I-cells become incoherent, which reduces, or even suppresses, the firing of the E-cells (Börgers and Kopell, 2005). For examples of parameter values for which this happens, see the paragraph on Fig. 1a in Appendix 2.

PING and Cell Assemblies

It has often been suggested that gamma rhythms are associated with the formation of “cell assemblies” (Singer and Gray, 1995). A cell assembly is a group of cells that are temporarily synchronous. Although synchrony can promote synaptic plasticity (Hebb, 1949), we will not assume that the cells are connected to one another. The suggestion is that temporary synchrony tags the neurons belonging to the assembly as working together and potentiates their down-stream effects.

When this hypothesis was first proposed, the gamma rhythm was thought to be relevant to binding partly because this frequency band had notably stronger power in situations in which such binding was seen to be important, such as early sensory processing (Gray, 1999). However, it was not clear what it was about this frequency band that should associate it with the creation of cell assemblies. A deeper understanding of the PING rhythm enables us to see why gamma and cell assemblies might indeed be related. The most relevant work is Olufsen et al. (2003). That paper considered an E/I network producing PING as described above, with the E-cells

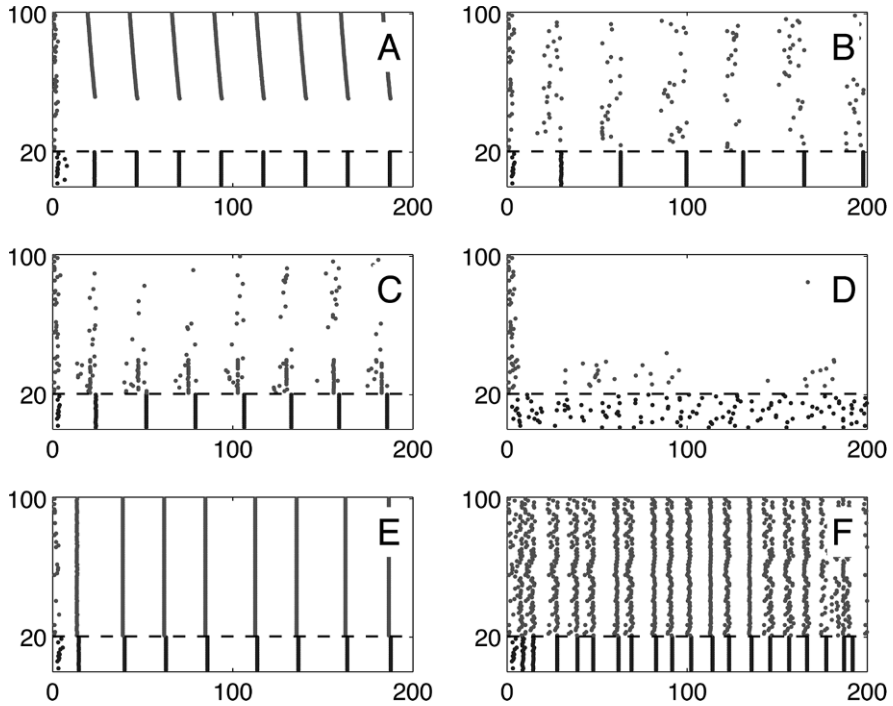


Fig. 1 Spike rastergrams of model E/I networks. Cells 1–20 (below the *dashed line*) are the I-cells, and cells 21–100 (above the *dashed line*) are the E-cells. **(a)** PING with heterogeneous input to the E-cells; strongly driven E-cells participate on every cycle, while weakly driven ones are suppressed altogether. **(b)** Weak PING driven by stochastic input to the E-cells. **(c)** Strong PING rhythm on a weak PING background. **(d)** Asynchronous activity of the I-cells at the same frequency as in panel C suppresses the E-cells. **(e)** E/I network entrained by sharp input pulses at gamma frequency; a strong but less coherent distractor was present as well, but its influence is not visible. **(f)** Without I→E synapses, the less coherent distractor prevents entrainment. All parameter values are given in Appendix 2

given a range of applied current, producing a range of natural frequencies for the individual cells. During PING, the E-cells with the highest drive fire with phases very close to one another, while the other E-cells are suppressed for the duration of the input. Thus, the cells that fire form a cell assembly; see also Fig. 1a of this chapter.

The dynamical reason for this behavior is found in the timing of the E- and (here, homogeneous) I-cells: when enough of the E-cells fire to cause the I-cells to fire, the resulting inhibition suppresses the rest of the E-cells. The fraction of cells firing depends on the kinetics and strength of the synapses and also on how the input is distributed across the E-cells. This fraction can be modulated by non-oscillatory inhibition, perhaps for instance from CCK-expressing cells (Tukker et al., 2007). The key point is that the same E-cells that fire on one gamma cycle fire again on the next, as long as the input to the cells remains the same. For this to happen, it

is critical that the decay time of inhibition is the longest time scale in the system. When this is true, by the time inhibition has worn off in a given gamma cycle, there is no cellular memory of which cells have spiked; thus, the same cells spike on each cycle, forming the cell assembly. If other currents with longer time scales (e.g., the M-current) are added, the cell assembly no longer forms. Instead, all the E-cells participate, at different times and at different frequencies (Olufsen et al., 2003).

Persistent Gamma

There is another kind of gamma in which the E-cells fire much less frequently than the population. This rhythm, known as “persistent gamma” or “weak gamma,” is formed in hippocampal slices by the addition of kainate and/or carbachol; for details, see chapter “Neuronal Activity Patterns During Hippocampal Network Oscillation In Vitro”. It is intrinsically more complex than ING and PING, since the firing of the E-cells seems stochastic. Indeed, the most detailed models of persistent gamma (Traub et al., 2000) require the existence of axo-axonal gap junctions among the pyramidal cells (Hamzei-Sichani et al., 2007). The axo-axonal connections give rise to very high-frequency (> 100 Hz) oscillations (VFOs) (Traub et al., 2000; Lewis and Rinzel, 2000, 2001; Munro, 2008), which are modulated by gamma frequency rhythms induced by the chemical synapses.

It might seem that the behavior of the resulting model cannot be captured by a less complicated model without the axonal plexus. However, it was shown by Börgers et al. (2005) that the noisy and low-frequency participation of the E-cells can be captured in a network of one-compartment E- and I-cells, without any axo-axonal interactions. This was done by replacing the noisy input to the E-cells generated within the axonal plexus by externally imposed noisy drive. We consider the gamma rhythm produced by this reduced network to have the same mechanism for the creation of the dynamics of the E/I interaction, but leaving out the details of how the network creates the necessary noise; see Fig. 1b for a rastergram of persistent gamma. We refer to this kind of rhythm as a “weak PING rhythm.” For clarity, we sometimes also call the standard, deterministically driven PING “strong PING.”

Local excitatory drive can generate a local PING rhythm on a background of persistent gamma (Börgers et al., 2005). The resulting acceleration of the inhibitory population leads to a reduction in activity of the non-assembly cells; see Fig. 1c. In order to form the cell assembly, it can in fact be critical that there be a background gamma: if this gamma is removed, for instance, by adding too much noise, weakening the I→E synapses too much, or giving extra drive to the I-cells, the same input to a subset of E-cells may not produce a cell assembly (Fig. 1d).

Gamma Rhythm and Protection Against “Distractors”

Synchrony does not require oscillations; a single common inhibitory input pulse, for instance, can produce it (Börgers and Kopell, 2003). However, the gamma rhythm is well-adapted biophysically to support the construction and use of cell assemblies

for several reasons. One such reason was discussed in Börgers and Kopell (2008) in the context of attention; although the assemblies were thought of as neocortical, similar issues pertain to the hippocampus, where cell assemblies have been recorded and analyzed (Harris et al., 2003). In Börgers and Kopell (2008), we considered a simple target network of one E- and one I-cell. The cells were coupled synaptically as in PING, but the target network did not fire in the absence of external input. The network received two rhythmic input trains at gamma frequency, a tightly coherent (“spiky”) one and a less coherent (more “sinusoidal”) one, both affecting the E- and the I-cell. The less coherent input train was faster or slower than the more coherent one, so that its effects on the target network could be distinguished, but both input frequencies were always in the gamma range.

Simulations showed, not surprisingly, that a single input entrained the target network. The more surprising result is that, in the presence of both input trains, the target network responded to the more coherent one, ignoring the less coherent one almost entirely, even when both input trains had the same temporal averages. The presence of the more coherent input made the less coherent input essentially invisible; see Börgers and Kopell (2008), and also Fig. 1e.

Further simulations and analysis showed that this effect depends on local inhibition within the target network; see Fig. 1f, in which the local inhibitory coupling has been removed, and the effect has disappeared. Inhibition greatly raises the leakiness of the target neurons; the more coherent input pulses can break through in spite of this leakiness, whereas the less coherent ones cannot (Börgers and Kopell, 2008). Once the coherent pulses entrain the target network, there is also a timing effect stabilizing the entrainment: the coherent pulses arrive at times when inhibition is weak, whereas the less coherent ones usually arrive at times when inhibition is stronger. The mechanism can work only at or above gamma frequency. At frequencies below the gamma range, there are substantial windows of low inhibition during which even the less coherent input can substantially affect the target network.

The Many Forms of Gamma, In Vitro and In Vivo

The relationship between in vitro and in vivo gamma rhythms is still not understood, though they are thought to be similar (Senior et al., 2008). Our current hypothesis is that the PING rhythm is associated with the formation of cell assemblies during active processing, and that the persistent rhythm is analogous to a background gamma rhythm associated with vigilance. Differences in frequencies may not point to differences between in vitro and in vivo mechanisms, since there is more background input in the in vivo structures. However, within in vitro varieties (as in CA3 or in CA1) the different frequencies may turn out to be salient. There are also differences in the gamma rhythms seen in vivo in a variety of structures. Recent work from the Graybiel lab (Tort et al., 2008) shows that different bands of gamma (30–60 Hz and 60–90 Hz) in the hippocampus are modulated differently by the theta rhythm, suggesting that they are mechanistically different. Work in the olfactory system (Kay, 2003) also suggests multiple gammas, a lower frequency one

associated with background attention, and a higher frequency one associated with active processing.

The distinctions between PING and persistent gamma do not adequately account for additional subtle differences seen even *in vitro*. For example, there are structure-dependent differences in gamma frequency, with CA3 *in vitro* persistent gamma slower than that of CA1 (Middleton et al., 2008). In the EC, there are two distinct gammas formed *in vitro*, associated with different kinds of interneurons; the slower one (in the 30 Hz range) is formed from an interaction of pyramidal cell with a class of interneurons named “goblet cells” (Middleton et al., 2008). It also remains to understand how other currents, not necessary for the existence of gamma rhythms, can nonetheless modulate them if they are present in high enough amounts. An example is the M-currents in the E-cells, which can affect the rate of firing of gamma or even make it disappear (Börgers et al., 2005; Olufsen et al., 2003). These subtleties may have important *in vivo* implications (Middleton et al., 2008).

Theta Rhythms

Unlike the gamma rhythm, which is governed (at least in its simplest forms) primarily by the decay time of inhibition, the theta rhythm seems to depend on the kinetics of intrinsic currents that determine the theta frequency or give rise to resonance at that frequency. Cells with intrinsic currents that may play a role in setting the theta frequency include the stellate cells of the EC and the O-LM cells in the hippocampus. For more information on the physiology and pharmacology of these and related cells, please see chapters “Neuronal Activity Patterns During Hippocampal Network Oscillation *In Vitro*” and “Single Neuron Models: Interneurons”.

Models of the Theta Rhythm in a Single Cell

The first physiological models of the theta rhythm were developed to describe the behavior of stellate cells of the EC (White et al., 1998b; Dickson et al., 2000; Acker et al., 2003). In these models, the time scale of the theta oscillation in an individual stellate cell comes from the interaction of a persistent Na^+ current with either a slow K^+ current (such as an M-current) or an h-current.

One outcome of modeling of the EC theta oscillations has been the suggestion that a geometric structure in the trajectories known as a “canard structure” is responsible for the theta period in subthreshold oscillations (Rotstein et al., 2006). The canard structure is related to the so-called canard phenomenon in which low amplitude oscillations blow up into large ones as some parameter is changed (Rotstein et al., 2006), which can occur when there are multiple time scales. In the canard structure, some trajectories follow repelling (unstable) manifolds for a significant amount of time, and that geometry determines the period of the oscillations for trajectories that stay close to oscillations for one or more cycles. In such a case, even when the oscillation has small amplitude, linearization around a fixed point does not

yield the period. This structure appears to affect resonance to theta-frequency input (Rotstein et al., unpublished observations).

A more detailed, multi-compartment model of an O-LM cell was created by Saraga et al., using the interaction of an h-current with an A-current, but no persistent Na^+ current (Saraga et al., 2003). The same group has more recently (Lawrence et al., 2006) incorporated the M-current into the model (chapter “Single Neuron Models: Interneurons”), and is currently modeling the R-LM cell (Chapman and Lacaille, 1999), making prominent use of the A-current. The different combinations of inward and outward currents have been shown to lead to some subtle differences in cellular dynamics (Acker et al., 2003). However, it is still not well understood how different combinations of currents lead to a propensity to produce subthreshold theta oscillations (Rotstein et al., 2006; Dickson et al., 2000) or respond in a resonant manner to inputs that have a theta-rich frequency distribution (Haas and White, 2002).

For the figures in this section, we will focus on a single-compartment version of the Saraga et al. model, which includes an h-current with a single time scale, and an A-current. The equations and all relevant parameters are in Appendix 1. We will refer to these model cells as O-cells. To put this model in context, we also describe related models below.

Synchronization Properties of Stellate Cells and O-LM Cells

The fact that single cells produce a given frequency does not imply that coupling those cells by their natural neurotransmitters will lead to a coherent rhythm. Previous modeling work on stellate cells and dynamic clamp experiments on stellate and O-LM cells illustrate this. Model stellate cells, coupled by AMPA synapses, do synchronize (Acker et al., 2003; Netoff et al., 2005a). This is counter to the results found earlier that simpler models of cells (integrate and fire or voltage-gated conductance with only spiking currents and leak) tend to synchronize with mutual inhibition, and not synchronize with excitation (van Vreeswijk et al., 1994; Gerstner et al., 1996). However, the addition of slower currents can change the synchronization properties. This is particularly true of the h-current and the M-current, both of which oppose applied currents (h-currents are inward currents that turn on with hyperpolarization, and M-currents are outward currents that turn on with depolarization) (Crook et al., 1998; Acker et al., 2003; Ermentrout et al., 2001). In addition to models cited above, this idea was tested by Netoff et al. (2005a), using the dynamic clamp method (Dorval et al., 2001; Sharp et al., 1993) on hybrid networks consisting of one stellate cell or O-LM cell, and one in silico (stellate) model of such a cell. The dynamic clamp could produce either excitation or inhibition in the hybrid network, and the results were compatible with the earlier modeling results: both stellate cell pairs and O-LM cell pairs can synchronize with excitation, but not with inhibition. Since the O-LM cells are inhibitory, this implies that a network of O-LM cells alone cannot produce a coherent theta rhythm. The results also suggested that, in spite of some differences in intrinsic currents between O-LM and stellate cells,

their synchronization properties are similar. Simulation of pairs of (reduced Saraga model) O-cells show that they also do not synchronize with inhibition (Pervouchine, unpublished).

There are various mathematical tools that are used to relate biophysical properties of cells to whether or not a pair of such cells can synchronize with a particular kind of synapse. More generally, the methods help decide and explain how a pair of cells phase-locks via the synaptic connection, and with what phase relationship (Kopell and Ermentrout, 2002). One such technique, emphasized in some of the examples mentioned above, involves “spike-time response curves” (STRCs) or, equivalently, “phase response curves” (PRCs) (Acker et al., 2003; Oprisan et al., 2004; Gutkin et al., 2005). In that methodology, one measures, from an experiment or in a numerical simulation (Galán et al., 2005; Netoff et al., 2005b), how much an input to a periodic cell changes the time of the next spike as a function of the time of the input (Fig. 2a). This change can be measured in time units (in STRCs) or in phase units (in PRCs), where phase usually represents the time normalized to the unperturbed, free-running period of the cell.

From the STRC, one can compute a “spike-time difference map” (STDM). The latter takes the time Δ in a given cycle between the spikes of the two cells and gives the time $\bar{\Delta} = \Delta + F(\Delta)$ between those spikes in the next cycle (Fig. 2b). Fixed points of that map (or, equivalently, zeroes of F) correspond to phase locking, and the slope of the map at the fixed point determines if the locking is stable to perturbations: stable phase locking occurs if and only if the slope of F is between -2 and zero. A fixed point with zero spike-time difference corresponds to synchrony; there is often another fixed point that (in a case of identical cells with symmetric coupling) corresponds to antiphase. If a fixed point is stable, its domain of stability (i.e., the set of initial phase lags which will lead to that fixed point) is the interval on either side of the fixed point up to the next fixed point; the sign of $F(\Delta)$ indicates whether the time lag between spikes will increase ($F(\Delta) > 0$) or decrease ($F(\Delta) < 0$) on the next cycle. An analog of STDM, which operates with phase instead of time, is called “phase transition map” (PTM). Note that the properties of locking regimes can be easily seen from STDM or PTM graphs, while the direct dynamic simulations convey information of a different sort, one that is more detailed but not as straightforward for the stability analysis.

The STRC and STDM connect physiological properties of the cells and synapses to the dynamical properties of the network of these cells, thus allowing one to understand how changes in some currents or time scales affect the network. For weak coupling, this theory is equivalent to the standard weak coupling theory (see Kopell and Ermentrout, 2002). But the theory can work for significantly larger coupling as well, and produces different answers. However, there are significant restrictions on the use of such methods: the major one is that the effect of the input of each cell on the other is assumed to happen within the current cycle, so that there is no further memory from one cycle to another. This can be relaxed to two cycles (Oprisan et al., 2004) and can deal with multiple inputs to the target (Netoff et al., 2005a). Another is that, in the most straightforward applications, the method applies to only two cells; this contrasts with weak coupling methods, in which an arbitrary number of cells can

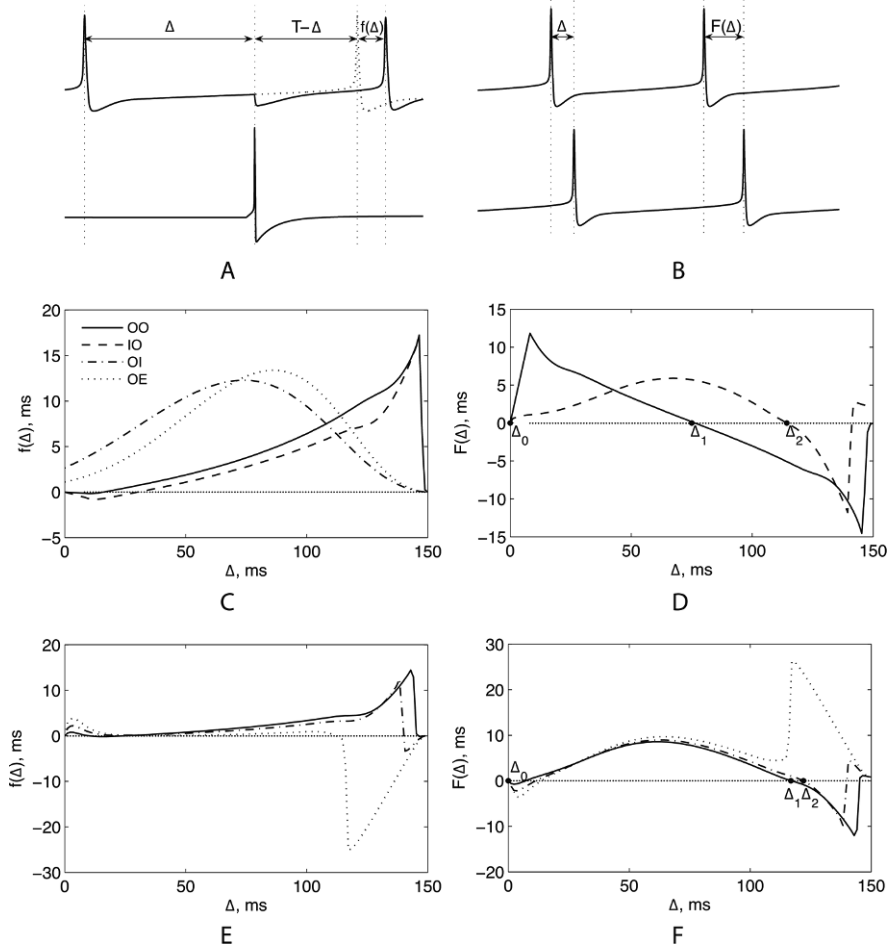


Fig. 2 (a) Construction of STRCs: Δ is the time of the perturbation; T is the unperturbed interspike interval; $f(\Delta)$ is the difference between the perturbed interspike interval and T . (b) Construction of STDMs: Δ and $F(\Delta)$ are time differences between spikes in two consecutive cycles. (c) STRCs for: an O-LM cell receiving input from another O-LM cell (*solid*); an O-LM cell receiving input from an I-cell (*dashed*); an I-cell receiving input from an O-LM cell (*dot-dashed*); an E-cell receiving input from an O-LM cell (*dotted*). Time units are normalized to the unperturbed period of 150 ms. (d) STDMs for: the network of mutually coupled O-LM cells (*solid*); the network of mutually coupled O-LM and I-cells (*dashed*). (e) STRCs for an O-LM cell receiving combined inhibitory and excitatory input from PING. The amount of inhibition is fixed, while excitation is used at three different levels: weak (*solid*), moderate (*dot-dashed*), and strong (*dotted*). (f) STDMs for the network of mutually coupled O-LM cell and E-I cell module (PING). *Line strokes* correspond to different levels of excitation, as in part e. All parameters for these simulations are given in Appendix 3

be combined in a network. The weak coupling hypothesis essentially assumes that all inputs to a cell are additive in their effects, an assumption that breaks down for non-linear coupling that is not infinitesimal. The method also assumes that the order of the cell spikes remains the same over different cycles.

Some of these constraints (notably, ones on time scales) are violated in our use of these methods. The 1-D reduction inherently involves a certain degree of inaccuracy since it neglects the dynamics of slow variables. While these effects are not noticeable for many simple Hodgkin–Huxley type of models, they can and do affect the Saraga O-LM cell model, which contains slow currents such as h-current or A-current. Nevertheless, the methods worked well for understanding synchronization of pairs of O-cells or stellate cells in the presence of inhibition or excitation, for reasons that may depend on further structure in the equations: we modeled how the resulting STRCs would change depending on the initial conditions of the slow variables and found that the dependence did not change the qualitative behavior, only the amplitude of STRCs. Although this could be broken by sufficiently large changes in the initial conditions of slow variables, we chose the initial values of gating variables close to those on the limit cycle, and the perturbations used to construct STRCs keep those slow variables within the range in which the quantitative behavior was not affected.

We now show how these ideas apply to a pair of mutually coupled O-cells. If we denote spike times of these cells by t_1 and t_2 , where $t_1 < t_2$, then on the next cycle the respective spike times will be $\bar{t}_1 = t_1 + T_O + f_{OO}(t_2 - t_1)$ and $\bar{t}_2 = t_2 + T_O + f_{OO}(\bar{t}_1 - t_2)$, where T_O is the period of a free-running O-cell, and $f_{OO}(\Delta)$ is the O-to-O STRC (Fig. 2c, solid line). The time difference between the two O-cells in the next cycle will be $\bar{\Delta} = \bar{t}_2 - \bar{t}_1 = \Delta + F_{OO}(\Delta)$, where $\Delta = t_2 - t_1$ and $F_{OO}(\Delta) = f_{OO}(T_O + f_{OO}(\Delta) - \Delta) - f_{OO}(\Delta)$. This function has two intercepts, one corresponding to synchronous, and another corresponding to antiphase oscillations (Fig. 2d, solid line). Standard theory of 1-D maps predicts that the synchrony (Δ_0) is unstable, while the antiphase locking regime (Δ_1) is stable, with domain of stability the entire period (this was confirmed in simulations). Thus, the O-cells do not synchronize with inhibition to produce the theta rhythm. Similar analyses made with other models of O-LM cells (Pervouchine et al., 2006) show qualitatively similar behavior.

Theta Rhythms in Hippocampal Networks

I-O Networks

In spite of the fact that the (model) O-LM cells do not synchronize with standard GABA_A inhibition, it is possible to have a theta rhythm in a network that is wholly inhibitory: Gillies et al. (2002) produced an atropine-sensitive theta rhythm in a CA1 slice in which glutamatergic synapses were blocked. In that experimental model, presumably there were multiple interneurons involved, in addition to the O-LM cells. Rotstein et al. (2005) produced a model of coherent theta in a network of

O-LM and basket (I) cells. Both types of cells were modeled as single compartment; and since the previous dynamic clamp work had suggested that the O-LM cells and EC stellate cells are biophysically similar in their synchronization properties, the 1-compartment models of the stellate cells were used. The frequency of the model cells was determined by the choice of the applied current (but see Goldin et al., 2007). The simplest such network model consisted of two Acker et al. models of the O-LM cell and one I-cell, with the former cells uncoupled, and the I-cell mutually coupled to each of the other two cells.

An essential hypothesis for this model is that I-cells, representing fast-firing interneurons (presumably parvalbumin-positive basket cells) do indeed receive inhibition from theta-producing cells such as the O-LM cells and vice versa. This has not been demonstrated anatomically or with paired cell recordings. However, in vitro, it has been seen that the O-LM cells display IPSPs with kinetics comparable to those of the FS cell, and basket cells display long IPSPs associated with the O-LM cells (Rotstein et al., 2005). There is also evidence that somatostatin-immunoreactive O-LM cells innervate distal apical dendrites of parvalbumin-positive basketed and/or axo-axonic interneurons (Katona et al., 1999, Fig. 7).

Analysis of how this synchronization works does not fit the standard uses of STRC and STDM, since the network has three cells. Nevertheless, it is possible to extend the analysis to this case. This was done in Pervouchine et al., (2006) for the Acker et al. model of the O-LM cell. The analysis done below illustrates the same results for the reduced Saraga et al. model (O-cells). Equations for O- and I-cells are in Appendix 1. The I-cells are as in previous sections.

A first step shows that, if the I-cells have weak enough drive to fire intrinsically in the theta-frequency range, each O-cell can phase-lock to the I-cell, at a phase such that the spike of the I-cell occurs relatively late in the O-cell cycle. This happens because the decay time of the inhibition induced by the O-LM cell is several times larger (20 ms) than that of the inhibition induced by basket cells (9 ms). Indeed, STRCs measuring the effects of the O- and the I-cell spikes on each other (Fig. 2c, dashed and dot-dashed lines) result in a STDM¹ that predicts stable non-synchronous oscillations (Δ_2 in Fig. 2d, dashed line).

The next step shows that, in the three cell network, the O-cells synchronize with each other because each synchronizes to the I-cell at the same phase. More specifically, if Δ is the time difference between spikes of the two O-cell and the I-cell spikes τ ms after the last of the two O-cells has spiked, then the time difference between the O-cells on the next cycle is $\bar{\Delta} = \Delta + F_{OO}(\Delta)$, where $F_{OO}(\Delta) = f_{IO}(\tau) - f_{IO}(\tau + \Delta)$ and $f_{IO}(\Delta)$ is the STRC function that models an input to the O-cell from an I-cell (Fig. 2c, dashed line). The synchronous solution is stable if $-2 < F'_{OO}(0) < 0$, i.e., if $0 < f'_{IO}(\tau) < 2$ (note that the derivative is with

¹ The derivation of STDM for the O-I network is very similar to that for the O-O network and yields $F_{OI}(\Delta) = f_{OI}(T + f_{IO}(\Delta) - \Delta) - f_{OI}(\Delta)$, where $f_{IO}(\Delta)$ and $f_{OI}(\Delta)$ are I-to-O and O-to-I STRCs shown in Fig. 2c (dashed and dot-dashed lines, respectively), and T is the unperturbed period of O- and I-cells.

respect to Δ). The latter condition holds for a relatively large range of values of τ , as shown by the dashed line in Fig. 2c.

We have shown that the entire O-I-O network can be regarded as a perturbation of an O-I network, in which the O-cells synchronize, provided that the I-cell does not spike shortly after one of the O-cells. In experimental observations and in the analysis done for the Acker et al. model (Pervouchine et al., 2006), this does not happen unless the decay time of the O-cells is set to be much longer than that of the I-cells. For the Saraga et al. model, the decay time of the O-cell inhibition does not have to be as long (Fig. 2c). The crucial distinction between the two models is that the Saraga et al. model has an A-current, which counterbalances the h-current and reduces the advance produced early in the cycle by the h-current in the Acker et al. model.

E-I-O Networks

There are several possible parameter regimes, producing theta frequency with different mechanisms. The central distinction is whether the O-cell fires as a result of excitation from the E-cell, or is held back by the inhibition from the I-cell (note that O-cells can also fire by post-inhibitory rebound, but this is more typical for the Acker et al. model rather than for the reduced Saraga model). Similar to what was described for O-I-O networks, a two-cell reduction is also possible for E-I-O networks, provided that the E-cell and the I-cell produce an oscillation of roughly the same frequency as does the O-cell. The dynamics are similar to PING, but at a lower frequency. (Without a model O-LM cell, this can lead to instability in the presence of noise; see Börgers and Kopell, 2005). The analysis of network dynamics then addresses the question of synchrony between the O-cell and either the E- or I-cells (the latter two cells spike almost synchronously and thus are referred to as an EI-module).

The combined effect of E- and I-cell spikes onto the O-cell can be regarded as a pulse that has both excitatory and inhibitory components. For simplicity, we change the excitatory conductance while keeping the amount of inhibition fixed; this results in a family of STRCs (depending on the excitatory conductance) from the EI-module to the O-cell, where the time of the perturbation is the time of the E-cell spike. (See Fig. 2e, where the different lines represent different strengths of the excitatory conductance). In turn, the O-cell spike impacts both E- and I-cells; here we use the assumption that the inhibitory feedback from the O-cell to the I-cell is negligible compared to the excitation, i.e., the E-to-I conductance is sufficient to make the I-cell fire independently of other inputs. The construction of the STDM is very similar to that in the O-O and O-I networks; the difference is only in the STRCs used.² The two functions needed to construct the STDM in this case are the O-to-E STRC (Fig. 2c, dotted line) and the EI-to-O STRC (Fig. 2e).

² In this case, the STRC is $F_{OE}(\Delta) = f_{OE}(T + f_{EI,O}(\Delta) - \Delta) - f_{OE}(\Delta)$, where $f_{OE}(\Delta)$ is the dotted line in Fig. 2c, and $f_{EI,O}(\Delta)$ is one of the functions shown in Fig. 2e.

The E-I-O network can oscillate in distinct modes (Fig. 2f). In the excitation-dominated regime (dotted line), the O-cell fires as a result of E-cell firing, in which case the zero phase lag between O- and E-cells (Δ_0) is the only fixed point, i.e., E, I, and O are roughly synchronous. In the inhibition-dominated regime (solid line), the O-cell phase-locks to the I-cell at a non-zero phase (Δ_1), as was observed in the O-I-O network, while the synchronous phase locking (Δ_0) has a tiny domain of stability. There is also a variety of intermediate regimes (dot-dashed line). In these regimes, additional (unstable) fixed points change the stability domains of Δ_0 and Δ_1 , thus providing a continuous transition between the two dominant regimes.

The distinction between “inhibition-dominated” and “excitation-dominated” versions of theta sheds light on the relationship to a theta rhythm model of Orban et al. (2006). Our inhibition-dominated model is based on Gillies et al.’s *in vitro* work, in which the AMPA receptors are blocked. This differs in some critical ways from the model of Orban et al., which also has pyramidal cells and two classes of inhibitory cells, basket cells, and O-LM cells. Unlike the models of this section, the Orban et al. model relies on the h-current in the pyramidal cells to promote rebound excitation; the firing of the pyramidal cells is critical for the creation of the model theta oscillation. Our “excitation-dominated” mechanism is also different from the Orban et al. model. In ours, the pyramidal cell is now crucial to the phases of the different kinds of cells, with the I- and O-cells roughly synchronous, but the theta frequency still comes from the properties of O-cells, not the h-current of the pyramidal cells. We also note that, in large-scale excitation-dominated models with the gamma rhythm nested in the theta rhythm (see section “Nested Gamma and Theta Rhythms”), the I-cells fire more often in parts of the theta cycle in which the O-cells are quiet, and hence *in vivo* measurements would indicate that I- and O-LM cells fire (statistically) at different times.

Nested Gamma and Theta Rhythms

As mentioned above and also reviewed elsewhere (chapter “Neuronal Activity Patterns During Hippocampal Network Oscillation *In Vitro*”), several *in vitro* pharmacological models have shown that the microcircuits of the hippocampus are able to generate theta and gamma rhythms locally (i.e., independently of an external pacemaker). It is also known that the co-existence of theta and gamma seen *in vivo* can be reproduced by certain protocols *in vitro* (Fisahn et al., 1998; Gillies et al., 2002; Gloveli et al., 2005b; Dugladze et al., 2007); i.e., there exists an intra-hippocampal mechanism for the coupling of gamma and theta rhythms. As in the sections above, many of the computational models built to date, including those reviewed here, were based on important *in vitro* results.

Inhibitory Networks

Both experiments and simulations show that a nested gamma and theta rhythm can occur in purely inhibitory networks (Gillies et al., 2002; Rotstein et al., 2005; Sereney, 2007). The same network that produces a theta rhythm with a coherent set

of O-cells can also produce a nested gamma rhythm inside the theta, provided that the I-cells have enough drive and that there are I-I synapses. This was shown for the Acker et al. model of O-LM cells in Rotstein et al. (2005). Figure 3a shows an example for the reduced Saraga et al. model (O-cells). In this situation, the mutual coupling of the model O-LM and I-cells is critical; a common input from the I-cells to the model O-LM cells, without O-I feedback, is not enough to synchronize the latter. Although each model O-LM cell adjusts its phase to the I-cell input, if the latter is much faster, the model O-LM cells skip I-cell cycles; the lack of synchronization is due to the fact that the different model O-LM cells skip different cycles. With mutual feedback between the I-cell and O-LM model cells (both models), the O-cells synchronize, with the I-cells forming a nested gamma (Fig. 3a).

If the synapses are strong, the standard STRC methods do not work well to explain this situation, even in a network of only one I- and one O-cell. The essential difficulty is that the inhibition from each successive spike of the I-cell in the O-cell network encounters a different set of O-cell conductances, since the currents in those cells are fairly long lasting. For both O-LM cell models, there are also large parameter regimes in which the number of I-spikes per O-cycle is erratic (P. Malerba, unpublished data). Simulations suggest that the erratic behavior may be related to trajectories passing nearby canards in the O-LM model equations.

A nested theta/gamma rhythm in a purely inhibitory network was also investigated numerically in White et al. (2000). In that set of simulations, there were again two kinds of interneurons, one with long IPSPs, and one with short ones. In contrast to the Rotstein et al. paper, the O-LM cell model had only spiking currents, no I_h , and there was a lot of heterogeneity in the drive to the cells. The network displayed gamma nested in theta, but not in a robust manner. The theta power went up with forcing at a theta frequency, and this was more effective, unintuitively, when the forcing was phase-dispersed. It is not fully understood how this resynchronization works. An analysis of a closely related system was given by Sereney (2007) for a single population of weakly driven interneurons. The synchronization was most effective when the weak periodic drive was close in frequency to the effective frequency of the network of interneurons. The analysis showed that the phase dispersion of the input changes that effective frequency by changing the number of interneurons that participate in the rhythm, recruiting more or suppressing more (see also Bathellier et al., 2008).

Since the gamma/theta behavior can be obtained with no intrinsic currents besides those needed for spiking, this raises the question of what role the special currents (I_A , I_h , maybe $I_{Na,P}$) play in these rhythms. For theta in a single cell, these currents are believed to be important for subthreshold oscillations (Dickson et al., 2000), and also for resonance (Hu et al., 2002; Haas and White, 2002). But it is less clear what roles these currents play in oscillatory regimes in which the O-LM cells spike. However, we note that the gamma/theta nesting in the White et al. (2000) model is not very robust without adding periodic input, and we conjecture that the time scales associated with the h-current and A-current are important in making these interactions more robust, probably by shaping the input resistance.

In fact, the result presented in Fig. 3a could not be achieved if the h- and A-currents were removed from the O-cell (after appropriate compensation of the drive current; data not shown), pointing to an important role of these currents for the coherence of the theta rhythm at the population level.

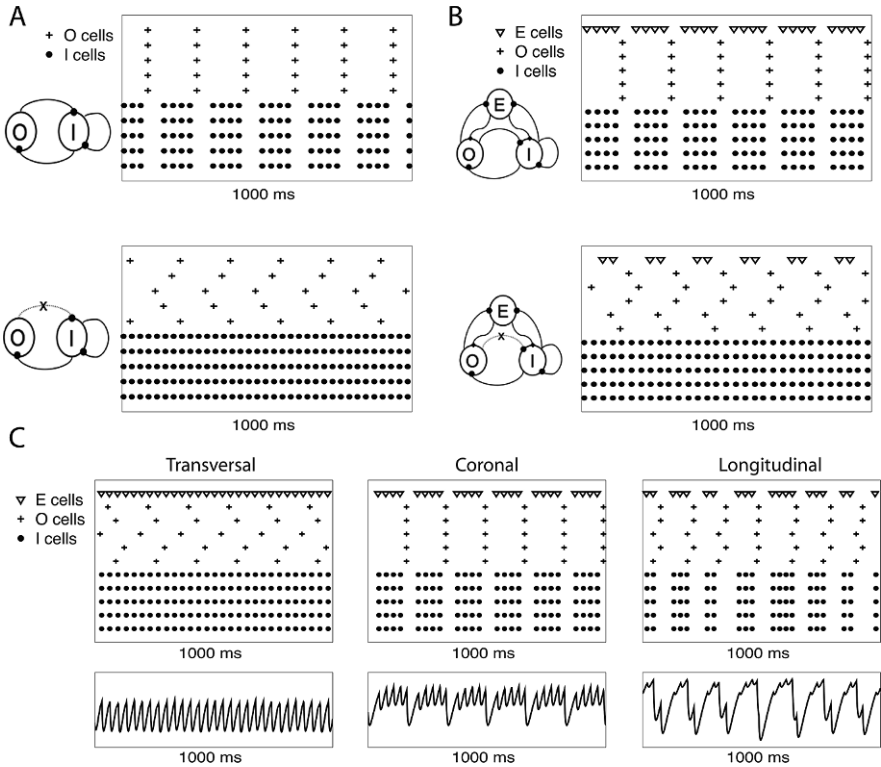


Fig. 3 Nested gamma and theta rhythms in simple hippocampal network models. **(a)** Pure inhibitory networks composed of I- and O-cells are able to generate coherent theta and gamma rhythms when the different cell types are mutually connected. Shown are the spike rastergrams for a network composed of 5 O- and 5 I-cells. The *bottom panel* shows a representative rastergram in the absence of O-I connections. In this case, although each individual O-cell spikes at theta frequency, the population of O-cells do not exhibit a coherent rhythm. Adding these connections, however, creates a coherent theta rhythm at the population level (*top panel*). **(b)** Theta and gamma rhythms in excitatory/inhibitory networks. Adding an E-cell to the network changes the type of gamma generation from ING to PING, i.e., the I-cells spike after the E-cell excitation. As shown for pure inhibitory networks, notice that a coherent theta rhythm is still dependent on the existence of O-I connections. **(c)** E-I-O network models of three hippocampal slice orientations. From transversal to longitudinal slices, O-cell connections (to all outputs) get stronger while I-cell connections get weaker, mimicking the orthogonal ramification property between these two interneurons (Gloveli et al., 2005b). The result is that the model LFP exhibits mostly gamma, mixed gamma/theta, or mostly theta oscillations in transversal, coronal, and longitudinal slices, respectively, as observed experimentally (Gloveli et al., 2005b). All parameter values are given in Appendix 4

Excitatory/Inhibitory Networks

In vivo, the networks producing the nested gamma/theta contain pyramidal cells as well as interneurons. Networks of pyramidal cells (E-cells), basket cells (I-cells), and O-LM cells (O-cells) were first studied in the context of in vitro work by Gloveli et al. on gamma and theta in CA3 (Gloveli et al., 2005b). In CA3, slices that are cut transversely and placed in an ACSF that contains kainate produce robust gamma rhythms (see chapter “Neuronal Activity Patterns During Hippocampal Network Oscillation In Vitro” for more details). If the slices are longitudinal, the same ACSF produces dynamics whose spectral content is mainly in the theta range; for a coronal slice, whose slice angle is in between, the spectral content has peaks in both the gamma and theta frequencies. The question addressed by the modeling is how different angles of the slice produce outputs with different frequency content.

The major difference between the three situations is in what part of the circuitry is preserved in the slices. The O-LM cells have long axons that project more in the longitudinal direction than in the transversal one (Gloveli et al., 2005b; Tort et al., 2007). Which connections are preserved in the transversal slice is not well understood: earlier studies suggested a lamellar organization of the hippocampus, in which the pyramidal cells would exert a greater influence in the transversal direction (Andersen et al., 1969, 2000), but this view has been challenged by other studies (Amaral and Witter, 1989; Wittner et al., 2007). More recently, however, it was shown that the gamma-producing basket cells do project more in the transverse direction (Gloveli et al., 2005b, see also Gloveli et al., 2005a). Thus, the longitudinal slice preserves more of the O-LM circuitry, and the transversal slice preserves more of the pyramidal-basket cell recurrent circuitry. We considered constructing a 3-D (or at least a 2-D) model in which that anatomy was explicitly modeled. Instead, we produced a more reduced description in which there was no explicit anatomy, but the preservation of more of the circuitry is modeled as a larger effect of those classes of cells. The O-LM cells are modeled by a 1-compartment reduction of the Saraga et al. model (O-cell), and the E- and I-cells are also modeled as in the previous sections; the one E-cell in the network is made to represent all the cells that are involved in a given cell population, while multiple I- and O-cells are used to explore issues of synchronization. We also employ a non-spiking E-cell as a caricature of a local field potential (LFP). This cell receives exactly the same synaptic inputs as the active E-cell in the network, but it is made silent by the absence of drive currents. The model LFP thus reflects subthreshold voltage changes in the E-cell population.

We first observe that such networks composed of E-I-O cells are able to produce nested gamma and theta oscillations (Fig. 3b). As in the case of pure inhibitory networks, O-I connections are required for a higher coherence of the theta rhythm by the O-cell population (Fig. 3b), and, likewise, removing I-O connections greatly reduces theta coherence (not shown). Next we study the effects of changing the strength of synaptic connections inside this network (Fig. 3c). The longitudinal slice is represented in this model by large O-I and O-E and lower I-O, I-I, and I-E conductances. The transverse slice has lower O-I and O-E and larger I-O, I-I, and I-E conductances, and the coronal slice has parameters in between. The results from these

simulations show behavior closely matching the experimental results: in the model transverse slice, the O-cells produce theta rhythms, not necessarily synchronized (given the low O-I synaptic conductance), and the E- and I-cells produce a PING rhythm. Given the strong I-E connections and the lack of coherence among O-cells, the model LFP exhibits mostly a gamma rhythm, as seen in the experiments. In the model longitudinal slice, the O-cells produce strong inhibition at theta frequency to both E- and I-cells. This is reflected in the model LFP, which shows mostly theta oscillations. The gamma rhythm is strongly reduced in the longitudinal slice model because of the large gap between the I-spikes (promoted by the long inhibition from the O-cells), together with a low I-E connection strength. In the coronal slice, where both interneurons present important influences over the E-cell population, the model LFP exhibits a clear nesting of the gamma and theta rhythm. Notice further that the gamma envelope (i.e., the amplitude of the gamma oscillation) is governed by the theta dynamics, which also matches experimental observations.

These observations have been reproduced in a more complex model in which there are many O- and I-cells, and the E-cell has five compartments, with the O-cell projecting to the distal dendrites, as in the actual anatomy (Tort et al., 2007). They also hold in models in which there are a large number of E-cells, and each E-cell fires at a low rate, while the population frequency is higher (e.g., persistent gamma for the transverse slice) (Tort et al., 2007).

We note that the present model differs from our previous modeling study of these phenomena (see Gloveli et al., 2005b). In our previous study, we also changed the strength of excitatory connections between the distinct slice angles. The main difference between the simulation results can be seen when comparing the longitudinal slice models: in Gloveli et al. (2005b) the low excitatory connections and strong inhibition by the O-cells impose a theta frequency for spikes in both the E- and I-cells, contrary to the present model. Whether there is such a difference in the frequency of spikes of basket and pyramidal cells between longitudinal and transversal slices remains to be studied experimentally; the two models make different predictions in this regard.

The simulation results give insight into recent *in vivo* work by the Monyer group in which the GABA_A receptors were knocked out in cells that are parvalbumin-positive (PV+), which include the fast-spiking basket cells (I-cells). Thus, in terms of the current model, the O-I and I-I connections are gone, but the O-cells and all the connections to them are preserved. The experiments showed that the gamma oscillation is preserved, but the theta oscillation is much reduced, as is the theta modulation of the gamma amplitude and frequency (Wulff et al., 2009). Indeed the latter is reduced beyond what is expected by the reduction of the theta amplitude (Wulff et al., 2009).

These results can be reproduced in the above networks (see the modeling study done in Wulff et al., 2009). In the larger E/I/O model with one E-cell, both the O-I and I-O connections are important for the production of a coherent theta oscillation. When the O-I connection is removed, the O-cells lose their coherence, as in the O/I model described above for the completely inhibitory theta rhythm. The theta power is reduced by the lack of coherence, and the theta modulation of gamma is reduced

further because the O-cells are no longer able to convey their theta rhythmicity to the I-cells, the cell type most critical for the gamma oscillation.

We note that the synapses from pyramidal cells to O-LM cells have been shown to be plastic, especially during the times that the O-LM cells are hyperpolarized (Oren et al., 2009). Thus, the parameter regimes may be subject to plastic changes.

Gamma/Theta and Cell Assemblies

Since gamma rhythms are associated with cell assemblies, and the O-LM cells extend across much of the longitudinal direction of the hippocampus, a natural question is whether the O-LM cells can help to coordinate the cells assemblies that the gamma rhythm helps to create. This question was addressed in Tort et al. (2007). The model used was a collection of modules with many E-, I-, and O-cells, each module a representation of a transversal slice. Each module has many O-, I-, and E-cells. The E-cells were multi-compartmental. This is important, since the O-LM cells project to the distal apical dendrites and the I-cells project more proximally, an anatomical arrangement that could potentially affect any coordination via the O-LM cells. The O-cells were connected to E-cells within a module and also, with a weaker synaptic strength, to E-cells of other modules. The full network had different anatomies, from nearest neighbor to multiple neighbors to all-all connections of modules, with or without conduction delays between modules. To test for the ability of the O-LM cells alone to create this coordination, we omitted any long excitatory connections. Indeed, we think of the connections from the O-cells to E-cells as hard wired, while the mutually excitatory connections can be formed plastically when the cells are part of a cell assembly; thus, the connectivity may change with experience.

The simulations showed that the O-LM cells alone can coordinate cell assemblies, and that the same theta rhythm can coordinate different cell assemblies with different frequencies in the gamma range (Tort et al., 2007; see also Fig. 4). Also, cell assemblies can be formed with only some of the E-cells in a participating module, depending on their level of excitation. As both O- and I-cells were phasically excited by the E-cells, gamma and theta frequencies move together as the drive to the pyramidal cells is changed, with a gamma/theta-frequency ratio roughly constant (Tort et al., 2007). The constancy of this ratio was shown in our models to be related to the dynamics of the excitation-dominated regime (see section “E-I-O Networks”).

The coordination of cell assemblies promoted by the O-cells was robust to changes in the conduction delays between modules compatible with the anatomy, and a little conduction delay actually provided tighter synchrony than none. The main drive to the E-cells in this model was considered to be derived from EC excitation and was therefore applied to the distal apical dendritic compartment. Interestingly, having the O-E synapse exactly at the same distal location as the E-cell drive led to higher robustness of the findings than an anatomical configuration having a perisomatic location of the O-E synapses. Also, the distal location of the drive to the E-cells makes the formation of inter-module gamma assemblies (promoted

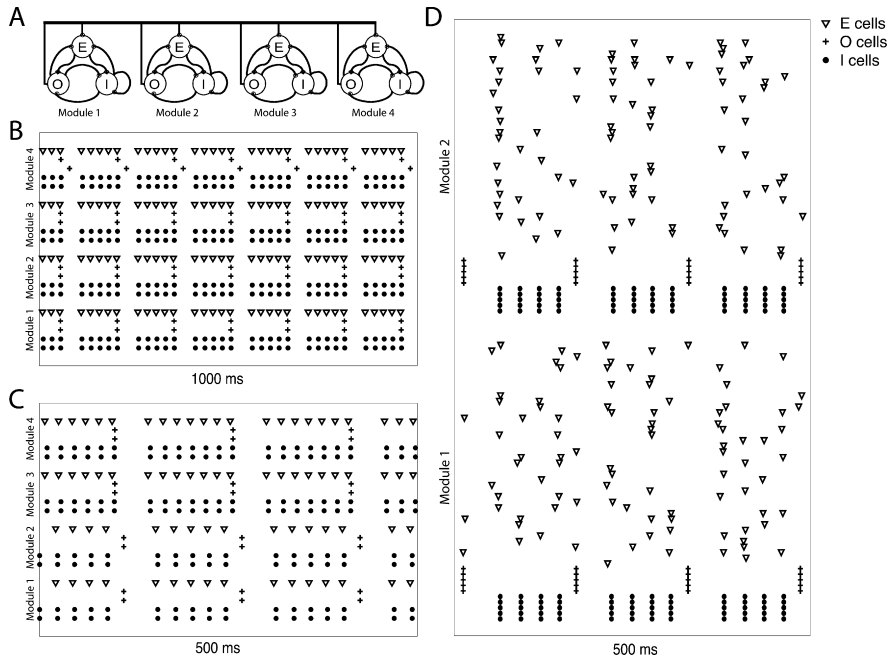


Fig. 4 O-LM cells can promote the formation of multiple gamma cell assemblies. **(a)** Multiple modules network scheme. Each module is composed of E-, I-, and O-cells (connected as in Fig. 3b top). Connections among modules are made only through O-E synapses, which is made to represent the larger axonal ramifications in the longitudinal direction of the hippocampus presented by the O-LM cells (Gloveli et al., 2005b; Tort et al., 2007). **(b)** Spike rastergram of a network composed of four modules (each module in the network is composed of 1 E-, 2 O-, and 2 I-cells), showing that O-LM cells are able to promote gamma synchrony among modules. **(c)** Same network as above, but with subsets of two modules excited with different E-cell drive levels. Note the formation of two gamma assemblies of distinct frequencies. **(d)** Spike rastergram of a network composed of two modules, with 40 E-, 5 O-, and 5 I-cells each. The network parameters are set so that each module exhibits weak PING (i.e., each E-cell spikes randomly and sparsely, below the gamma frequency, but the E-cell population still exhibits gamma; see also Fig. 1b). The O-LM cells are also able to promote gamma synchrony among modules under this regime. All parameter values for these simulations are given in Appendix 4

by the O-cells) more robust to distinct levels of excitation among E-cells. This robustness is related to the A-current, which is higher at the pyramidal cell dendrites and flattens the spiking frequency vs. applied drive (F-I) curve. The flatter F-I curve allows more coordination for the same amount of drive heterogeneity when compared to the somatic location of the drive currents. The modeling suggests that this circuit is well organized to coordinate and form gamma cell assemblies from EC inputs.

Although the use of a multi-compartmental model in the previous study provided insights about the functional architecture of this microcircuit and its multiple participating currents, in Fig. 4 we show that the formation of gamma assemblies

promoted by O-cells is robust enough to hold with simpler models of pyramidal cells; for instance, all the results in this figure were obtained by using the same E-, I-, and O-cell models as in the other sections of this chapter.

Conclusions and Future Directions

The model networks described here are very simple approximations of the actual biological systems. Nevertheless, we believe that their analysis constitutes an important attempt to gain further knowledge about the possible biophysical mechanisms underlying hippocampal oscillations as well as about their potential functions. The aim is to capture what is essential to produce the rhythms and their interactions.

There are many future directions for the work presented above. The current work considers the formation of gamma and theta rhythms, their interactions, and their roles in the formation and coordination of cell assemblies. Challenging questions that can build upon the current work include how the multiple inputs from the EC, the septal nucleus, and other structures can be integrated within CA3 and CA1 to produce associations of memories occurring simultaneously and in sequences (Dragoi and Buzsáki, 2006; Senior et al., 2008; Pastalkova et al., 2008; Itskov et al., 2008). It is likely that other kinds of interneurons known to fire at different phases in the theta rhythm (Klausberger et al., 2003) will be important for such extensions. We believe that an understanding of how the physiology and anatomy of the cells and circuits give rise to the rhythms of the hippocampus provides central clues to how the hippocampus makes use of these dynamics in learning and recall.

Appendix 1: Neuronal and Synaptic Models

Pyramidal cells: We use the pyramidal cell model of Olufsen et al. (2003):

$$C \frac{dV}{dt} = g_{\text{Na}} m_{\infty}(V)^3 h (V_{\text{Na}} - V) + g_{\text{K}} n^4 (V_{\text{K}} - V) + g_{\text{L}} (V_{\text{L}} - V) + I \quad (1)$$

$$\frac{dh}{dt} = \frac{h_{\infty}(V) - h}{\tau_h(V)} \quad (2)$$

$$\frac{dn}{dt} = \frac{n_{\infty}(V) - n}{\tau_n(V)} \quad (3)$$

with

$$x_{\infty}(V) = \frac{\alpha_x(V)}{\alpha_x(V) + \beta_x(V)} \quad \text{for } x = m, h, \text{ or } n \quad (4)$$

$$\tau_x(V) = \frac{1}{\alpha_x(V) + \beta_x(V)} \quad \text{for } x = h \text{ or } n \quad (5)$$

$$\alpha_m(V) = \frac{0.32(V + 54)}{1 - \exp(-(V + 54)/4)}$$

$$\begin{aligned}\beta_m(V) &= \frac{0.28(V + 27)}{\exp((V + 27)/5) - 1} \\ \alpha_h(V) &= 0.128 \exp(-(V + 50)/18) \\ \beta_h(V) &= \frac{4}{1 + \exp(-(V + 27)/5)} \\ \alpha_n(V) &= \frac{0.032(V + 52)}{1 - \exp(-(V + 52)/5)} \\ \beta_n(V) &= 0.5 \exp(-(V + 57)/40)\end{aligned}$$

In Eqs. (1), (2), and (3), the letters C , V , t and τ , g , and I denote capacitance density, voltage, time, conductance density, and current density, respectively. The units that we use for these quantities are $\mu\text{F}/\text{cm}^2$, mV, ms, mS/cm^2 , and $\mu\text{A}/\text{cm}^2$. For brevity, units will usually be omitted from here on. The parameter values of the model are $C = 1$, $g_{\text{Na}} = 100$, $g_{\text{K}} = 80$, $g_{\text{L}} = 0.1$, $V_{\text{Na}} = 50$, $V_{\text{K}} = -100$, and $V_{\text{L}} = -67$.

This model is a variation on one proposed by Ermentrout and Kopell (1998); the difference is that in Ermentrout and Kopell (1998), the gating variable h was taken to be a function of n . The model of Ermentrout and Kopell (1998), in turn, is a reduction of a model due to Traub and Miles (1991).

Fast-spiking interneurons: For fast-spiking interneurons, we use the Wang and Buzsáki (1996) model. Equations (1), (2), (3), and (4) are as in the pyramidal cell model. Equation (5) is replaced by

$$\tau_x(V) = \frac{0.2}{\alpha_x(V) + \beta_x(V)} \text{ for } x = h \text{ or } n \quad (5)$$

The rate functions α_x and β_x , $x = m, h$, and n , are defined as follows:

$$\begin{aligned}\alpha_m(V) &= \frac{0.1(V + 35)}{1 - \exp(-(V + 35)/10)} \\ \beta_m(V) &= 4 \exp(-(V + 60)/18) \\ \alpha_h(V) &= 0.07 \exp(-(V + 58)/20) \\ \beta_h(V) &= \frac{1}{\exp(-0.1(V + 28)) + 1} \\ \alpha_n(V) &= \frac{0.01(V + 34)}{1 - \exp(-0.1(V + 34))} \\ \beta_n(V) &= 0.125 \exp(-(V + 44)/80)\end{aligned}$$

The parameter values, using the same units as for the pyramidal cells, are $C = 1$, $g_{\text{Na}} = 35$, $g_{\text{K}} = 9$, $g_{\text{L}} = 0.1$, $V_{\text{Na}} = 55$, $V_{\text{K}} = -90$, and $V_{\text{L}} = -65$.

O-LM interneurons: For the oriens lacunosum-moleculare interneurons, we use the model described in Tort et al. (2007), which is a reduction of the multi-compartmental model described in Saraga et al. (2003). The current-balance equation is given by

$$C \frac{dV}{dt} = g_{\text{Na}} m^3 h (V_{\text{Na}} - V) + g_{\text{K}} n^4 (V_{\text{K}} - V) + g_{\text{A}} a b (V_{\text{A}} - V) + g_{\text{h}} r (V_{\text{h}} - V) + g_{\text{L}} (V_{\text{L}} - V) + I \quad (6)$$

with

$$\frac{dx}{dt} = \frac{x_{\infty}(V) - x}{\tau_x(V)} \text{ for } x = m, h, n, a, b, r \quad (7)$$

For $x = m, n, h$, the functions $x_{\infty}(V)$ and $\tau_x(V)$ are the same as in (4) and (5), and the rate functions α_x and β_x are defined as follows:

$$\begin{aligned} \alpha_m(V) &= \frac{-0.1(V + 38)}{\exp(-(V + 38)/10) - 1} \\ \beta_m(V) &= 4 \exp(-(V + 65)/18) \\ \alpha_h(V) &= 0.07 \exp(-(V + 63)/20) \\ \beta_h(V) &= \frac{1}{1 + \exp(-(V + 33)/10)} \\ \alpha_n(V) &= \frac{0.018(V - 25)}{1 - \exp(-(V - 25)/25)} \\ \beta_n(V) &= \frac{0.0036(V - 35)}{\exp((V - 35)/12) - 1} \end{aligned}$$

For $x = a, b, r$, we provide the functions $x_{\infty}(V)$ and $\tau_x(V)$ below:

$$\begin{aligned} a_{\infty}(V) &= \frac{1}{1 + \exp(-(V + 14)/16.6)} \\ \tau_a(V) &= 5 \\ b_{\infty}(V) &= \frac{1}{1 + \exp((V + 71)/7.3)} \end{aligned}$$

$$\tau_b(V) = \frac{1}{\frac{0.000009}{\exp((V-26)/18.5)} + \frac{0.014}{0.2 + \exp(-(V+70)/11)}}$$

$$r_\infty(V) = \frac{1}{1 + \exp((V + 84)/10.2)}$$

$$\tau_r(V) = \frac{1}{\exp(-14.59 - 0.086V) + \exp(-1.87 + 0.0701V)}$$

The parameter values are $C = 1.3$, $g_L = 0.05$, $g_{Na} = 30$, $g_K = 23$, $g_A = 16$, $g_h = 12$, $V_{Na} = 90$, $V_K = -100$, $V_A = -90$, $V_h = -32.9$, $V_L = -70$.

Synaptic model: We adopt the synaptic model of Ermentrout and Kopell (1998).³ Each synapse is characterized by a synaptic gating variable s associated with the presynaptic neuron, with $0 \leq s \leq 1$. This variable obeys

$$\frac{ds}{dt} = \rho(V) \frac{1-s}{\tau_R} - \frac{s}{\tau_D}$$

where ρ denotes a smoothed Heaviside function:

$$\rho(V) = \frac{1 + \tanh(V/4)}{2}$$

and τ_R and τ_D are the rise and decay time constants, respectively. To model the synaptic input from neuron i to neuron j , we add to the right-hand side of the equation governing the membrane potential V_j of neuron j a term of the form

$$g_{ij}s_i(t)(V_{\text{rev}} - V_j)$$

where g_{ij} denotes the maximal conductance associated with the synapse, s_i denotes the gating variable associated with neuron i , and V_{rev} denotes the synaptic reversal potential. For AMPA receptor-mediated synapses, we use $\tau_R = 0.1$, $\tau_D = 3$, and $V_{\text{rev}} = 0$; for GABA_A receptor-mediated synapses, $\tau_R = 0.3$, $\tau_D = 9$, and $V_{\text{rev}} = -80$, if the synapse originates from a basket cell, and $\tau_R = 0.2$, $\tau_D = 20$, and $V_{\text{rev}} = -80$, if it originates from an O-LM cell.

³ The models presented in section “Nested Gamma and Theta Rhythms” use the NEURON built-in function *Exp2Syn()* for modeling the synaptic gating variable s , which takes as parameters the rise and decay time constants. This is a double exponential function that is close to, but not identical with, the function s described here.

Appendix 2: Parameter Values in Section “Gamma Rhythms, in Various Guises”

Here we specify the parameter values used in the simulations of Fig. 1, and briefly discuss how variations in these values would affect the results. We have also included with the code the six parameter files which produce the panels of Fig. 1.

Notation: We denote by N_E and N_I the numbers of E- and I-cells, respectively. We take the maximal conductance of the synaptic connection from the i th I-cell to the j th E-cell to be

$$X_{IE,ij} \frac{\hat{g}_{IE}}{p_{IE}N_I}$$

with $\hat{g}_{IE} \geq 0$, $0 < p_{IE} \leq 1$, and

$$X_{IE,ij} = \begin{cases} 1 & \text{with probability } p_{IE}, \\ 0 & \text{with probability } 1 - p_{IE} \end{cases}$$

where $p_{IE}N_I$ is the expected number of I-cells from which an E-cell receives synaptic input, and \hat{g}_{IE} is the expected value of the maximal total inhibitory conductance affecting an E-cell. Similar formulas are used for the E→I, I→I, and E→E synapses. The random variables $X_{IE,ij}$, $X_{EI,ij}$, $X_{II,ij}$, and $X_{EE,ij}$ are assumed to be independent.

The external drive has deterministic and stochastic components. The deterministic drive (“ I ” in Eq. (1) of Appendix 1) is $I_{E,i}$ for the i th E-cell and $I_{I,i}$ for the i th I-cell. The stochastic component of the drive to a cell is modeled by an additional term on the right-hand side of Eq. (1), of the form $-s_{\text{stoch}}(t) g_{\text{stoch}} V$. The gating variable s_{stoch} decays exponentially with time constant $\tau_{D,\text{stoch}}$ during each time step. At the end of each time step, s_{stoch} jumps up to 1 with probability $\Delta t f_{\text{stoch}}/1000$. This simulates the arrival of external synaptic input pulses. The mean frequency with which input pulses arrive is f_{stoch} . Even though we measure time in ms, we measure frequencies in Hz = s⁻¹; this unit, like the others, will usually be omitted from here on. Different cells in the network receive independent stochastic input streams. We use subscripts E and I to label the values of g_{stoch} , f_{stoch} , and $\tau_{D,\text{stoch}}$ for the E- and I-cells, respectively; for instance, the value of g_{stoch} for the E-cells is $g_{\text{stoch},E}$.

Numerics: The simulations shown in Fig. 1 were carried out using the midpoint method with $\Delta t = 0.02$. Results obtained with smaller values of Δt were not significantly different.

Parameter values common to all panels of Fig. 1: $N_E = 80$ and $N_I = 20$. Since we scale the excitatory and inhibitory synaptic conductances by N_E and N_I , respectively, the network size does not affect the results much. Connectivity is all-to-all: $p_{EE} = p_{EI} = p_{IE} = p_{II} = 1$. Plots similar to those of Fig. 1 are also obtained with sparse, random connectivity, provided that each I-cell receives input from sufficiently many E-cells, and vice versa (Börgers and Kopell, 2003; Golomb and

Hansel, 2000). The synaptic rise and decay time constants and reversal potentials are as specified in Appendix 1. Variations in the rise time constants, and in the decay time constant $\tau_{D,E}$ of excitation can have effects similar to those of variations in synaptic strengths (see below). The decay time constant $\tau_{D,I}$ of inhibition is a crucial factor in determining the frequency of the rhythms of panels A through C: the oscillation period depends on it linearly. The reversal potential of the excitatory synapses, $V_{\text{rev},E} = 0$, does not much affect the simulations of Fig. 1. However, if the reversal potential of inhibitory synapses, $V_{\text{rev},I} = -80$, is raised (for instance, to -65 , modeling inhibition that is shunting rather than hyperpolarizing), gamma frequency rhythms are obtained only if the external drive to the E-cells is lowered, or the I→E synapses strengthened. There are no E→E synapses in Fig. 1: $\hat{g}_{EE} = 0$. Such synapses can raise the number of E-cells participating in each population spike volley; for instance, with $\hat{g}_{EE} = 0.5$, no E-cells would be suppressed in Fig. 1a, and the weak PING rhythm of Fig. 1b would turn into strong PING.

Specific parameter values for the six panels:

Panel A: (strong PING) $\hat{g}_{EI} = 0.5$, $\hat{g}_{IE} = 1.5$, $\hat{g}_{II} = 0.5$, $I_{E,i} = 2.5 + 2i/N_E$ for the i th E-cell (cell number $20+i$ in Fig. 1), $g_{\text{stoch},E} = 0$, $I_{I,i} = 0$, $g_{\text{stoch},I} = 0$. All parameters can be varied considerably without losing the PING rhythm. When \hat{g}_{EI} is raised, the spiking of the E-cells triggers the response of the I-cells more promptly; as a result, more E-cells are suppressed. In agreement with analysis (Börgers and Kopell, 2003), the population period T depends logarithmically on \hat{g}_{IE} ($T = 23.4, 29.4, 35.4$ for $\hat{g}_{IE} = 1.5, 3, 6$), and linearly on $\tau_{D,I}$ ($T = 23.4, 29.1, 34.6$ for $\tau_{D,I} = 9, 12, 15$). The external drive I_E must be strong enough to drive the E-cells at an *intrinsic frequency* (the frequency that would be obtained in the absence of any synaptic connections) in or above the gamma range (Börgers and Kopell, 2003). In Fig. 1a, the intrinsic frequencies of the E-cells vary between 80 Hz ($I_E = 2.5$) and 120 Hz ($I_E = 4.5$). Strong drive to the I-cells abolishes the rhythm. Under idealized circumstances, there is a sharp threshold value of I_I above which the rhythm is lost (Börgers and Kopell, 2005). In a more realistic network, the threshold is not sharp, but the transition can be fairly rapid (Börgers et al., 2008). For instance, there is a PING rhythm very similar to that in Fig. 1a if $I_{I,i} = 1.5 + i/N_I$, but for $I_{I,i} = 2.0 + i/N_I$, the I-cells spike largely asynchronously, and the E-cells are suppressed. The PING rhythm can be protected against the effects of external drive to the I-cells by raising \hat{g}_{II} (Börgers and Kopell, 2005).

Panel B: (weak PING) Much of the external drive to the E-cells is stochastic in Fig. 1b: $I_{E,i} = 1.25$, $g_{\text{stoch},E} = 0.1$, $f_{\text{stoch},E} = 20$, $\tau_{D,\text{stoch},E} = 3$ (the decay time constant of AMPA receptor-mediated synapses), all other parameters as for Fig. 1a. The properties of weak PING rhythms and their parameter dependence require further study. However, as one would expect, the frequency is a decreasing function of $\tau_{D,I}$ and \hat{g}_{IE} . It is an increasing function of $f_{\text{stoch},E}$,

though the dependence is surprisingly weak. (See Figs. 4 and 6 of Reinker et al. (2006) for a similar observation.)

Panel C: (strong PING on a weak PING background) $I_{E,i} = 3.25$ for the first 20 E-cells (cells 21 through 40 in Fig. 1), all other parameters as in panel B.

Panel D: (asynchronous I-cells suppress E-cells) All synaptic inputs to the I-cells are removed here ($\hat{g}_{EI} = \hat{g}_{II} = 0$), replaced by strong, brief stochastic input pulses, forcing the I-cells to spike stochastically at approximately 38 Hz (the frequency of the I-cells in panel C): $g_{\text{stoch},I} = 0.5$, $f_{\text{stoch},I} = 38$, $\tau_{D,\text{stoch},I} = 1$. All other parameters are as in panel C.

Panel E: (entrainment by a 40-Hz sequence of tight input pulses, in the presence of a competing 56-Hz sequence of broader pulses) All parameters as in panel A, except $I_{E,i} = 4 \sin^8(40\pi t/1,000) + 4 \sin^2(56\pi t/1,000)$.

Panel F: All parameters as in panel E, except $\hat{g}_{IE} = 0$.

Appendix 3: Parameter Values in Section “Theta Rhythms”

Below we describe the protocol used to construct spike-time response curves (STRCs) and spike-time difference maps (STDMs). We also specify the parameter values used in Fig. 2.

The dynamical models of cells and synapses are given in Appendix 1. To construct a phase response curve, two cells (referred to as presynaptic cell and postsynaptic cell, respectively) were connected by a synapse. The synaptic conductance is denoted by g_{XY} , where X is the presynaptic and Y is the postsynaptic cell. The period of each postsynaptic cell was set to approximately 150 ms by using the corresponding value of the DC current ($I_{\text{app}} = 0.137$ for pyramidal cells, $I_{\text{app}} = 0.185$ for fast-spiking interneurons, and $I_{\text{app}} = -4.70$ for O-LM interneurons). Presynaptic cells were set not to spike using appropriate DC currents. The postsynaptic cell was run for three full periods to make the values of gating variables close to those on the limit cycle. At that, the dynamical models of pyramidal cells and fast-spiking interneurons approach their limit cycles well enough regardless of initial conditions. The initial values of gating variables for the Saraga O-LM cell model, which contains slow currents such as h-current and A-current, were as follows: $V = -75.61$, $m = 0.0122$, $n = 0.07561$, $h = 0.9152$, $r = 0.06123$, $a = 0.0229$, $b = 0.2843$.

At time t , the presynaptic cell was given a short (3 ms) DC current pulse to trigger exactly one spike, and the effect of this spike on the spike time of the postsynaptic cell was measured (we define the time of the spike as the midpoint between the two time points at which the membrane potential crosses the +10 mV threshold). Denote by t_0 and t_2 the spike times of the postsynaptic cell in two consecutive periods and

assume that the presynaptic cell spikes at time t_1 ($t_0 < t_1 < t_2$). Note that the presynaptic cell spikes shortly after, but not at the same time as the DC pulse arrives, i.e., $t_1 > t$. We define the spike-time response function as $f(\Delta) = t_2 - t_0 - T$, where $\Delta = t_1 - t_0$ and $T = 150$ ms. This procedure was repeated for different values of t with the time increment of 1 ms and yielded the values of $f(\Delta)$ on a uniform grid of Δ ($0 < \Delta < T$). Additionally, we define $f(0) = f(T) = 0$.

The synaptic conductances used in Fig. 2c were $g_{OO} = 0.09$, $g_{IO} = 0.30$, $g_{OI} = 0.002$, and $g_{OE} = 0.002$. Spike time difference maps in Fig. 2d were constructed as explained in section “Theta Rhythms” using linear interpolation of STRCs shown in Fig. 2c. To construct PING-to-O STRCs (Fig. 2e), we created a PING network by connecting one pyramidal cell (E) and one fast-spiking interneuron (I); the synaptic conductances were $g_{IE} = 0.4$, $g_{EI} = 0.2$, and $g_{II} = 0.3$, where g_{II} is an autapse. At that, a short DC current pulse to the E-cell triggered exactly one spike and, through synaptic excitation, exactly one spike of the I-cell. The effect of the combined excitatory and inhibitory inputs to the O-cell was measured by the function $f_{EI,O}(\Delta)$ shown in Fig. 2e. The PING module was connected to an O-cell by using $g_{IO} = 0.2$ and three levels of excitatory conductance: $g_{EO} = 0.04$, $g_{EO} = 0.08$, and $g_{EO} = 0.14$ (solid, dot-dashed, and dotted traces in Fig. 2e). STDMs in Fig. 2f were constructed by using the corresponding STRCs from Figs. 2c and 2e.

Appendix 4: Parameter Values in Section “Nested Gamma and Theta Rhythms”

Here we specify the parameter values used in the simulations of Figs. 3 and 4. All these simulations were performed using the software NEURON (Hines and Carnevale, 1997), which is available for free download.⁴

Notation: We denote by N_E , N_I , and N_O the numbers of E-, I-, and O-cells inside a module, respectively. The maximal conductance of the synaptic connection from the cell type X to cell type Y is given by⁵

$$G_{XY} = \frac{\hat{g}_{XY}}{N_X}, \quad X, Y = O, I, E.$$

We denote by I_X the drive current to cell type X ($X = O, I, E$). Below we report the values employed for \hat{g}_{XY} and I_X in each figure, panel by panel. Any parameter not explicitly specified has value equal to zero.

⁴ <http://www.neuron.yale.edu/neuron/> and <http://neuron.duke.edu/>

⁵ Note that the normalization is only made for the number of cells within one module, and, in particular, it does not take into consideration the number of modules in the network.

Figure 3:

Panel A: Top panel: $\hat{g}_{II} = 0.1$, $\hat{g}_{OI} = 0.2$, $\hat{g}_{IO} = 0.5$, $I_I = 1$, $I_O = -3$. In the bottom panel, \hat{g}_{OI} was set to zero.

Panel B: Top panel: $\hat{g}_{II} = 0.1$, $\hat{g}_{OI} = 0.2$, $\hat{g}_{IO} = 0.5$, $\hat{g}_{IE} = 0.1$, $\hat{g}_{OE} = 0.15$, $\hat{g}_{EI} = 0.05$, $\hat{g}_{EO} = 0.01$, $I_E = 0.8$, $I_I = 0.8$, $I_O = -3$. In the bottom panel, \hat{g}_{OI} was set to zero.

Panel C: Left panel: $\hat{g}_{II} = 0.13$, $\hat{g}_{OI} = 0.03$, $\hat{g}_{IO} = 0.7$, $\hat{g}_{IE} = 0.15$, $\hat{g}_{OE} = 0.03$, $\hat{g}_{EI} = 0.05$, $\hat{g}_{EO} = 0.01$, $I_E = 0.8$, $I_I = 0.8$, $I_O = -3$. Middle panel: $\hat{g}_{II} = 0.1$, $\hat{g}_{OI} = 0.15$, $\hat{g}_{IO} = 0.5$, $\hat{g}_{IE} = 0.08$, $\hat{g}_{OE} = 0.15$, $\hat{g}_{EI} = 0.05$, $\hat{g}_{EO} = 0.01$, $I_E = 0.8$, $I_I = 0.8$, $I_O = -3$. Right panel: $\hat{g}_{II} = 0.05$, $\hat{g}_{OI} = 0.3$, $\hat{g}_{IO} = 0.2$, $\hat{g}_{IE} = 0.02$, $\hat{g}_{OE} = 0.3$, $\hat{g}_{EI} = 0.05$, $\hat{g}_{EO} = 0.01$, $I_E = 0.8$, $I_I = 0.8$, $I_O = -3$.

Figure 4:

Panel B: $\hat{g}_{II} = 0.1$, $\hat{g}_{OI} = 0.2$, $\hat{g}_{IO} = 0.5$, $\hat{g}_{IE} = 0.1$, $\hat{g}_{OE} = 0.1$, $\hat{g}_{EI} = 0.1$, $\hat{g}_{EO} = 0.01$, $I_E = 1.3$ (all modules), $I_I = 0.8$, $I_O = -1$. We set $\hat{g}_{OE} = 0.08$ among modules, with a 3-ms conduction delay among modules.

Panel C: Same parameters as in Panel B, except that Modules 1 and 2 had $I_E = 1.4$, whereas $I_E = 2$ in Modules 3 and 4.

Panel D: $\hat{g}_{II} = 0.1$, $\hat{g}_{OI} = 0.2$, $\hat{g}_{IO} = 0.5$, $\hat{g}_{IE} = 0.1$, $\hat{g}_{OE} = 0.6$, $\hat{g}_{EI} = 0.2$, $\hat{g}_{EO} = 0.05$, $I_E = 0.5 + W$ (all modules), where W is a white noise process with $\text{Var} = 0.02$, $I_I = 1$, $I_O = -2$. We set $\hat{g}_{OE} = 0.06$ among modules, with a 3-ms conduction delay among modules.

Further Reading

- Acker, C. D., Kopell, N., and White, J. A. 2003. Synchronization of strongly coupled excitatory neurons: relating network behavior to biophysics. *J Comput Neurosci*, 15, 71–90.
- Amaral, D. G., and Witter, M. P. 1989. The three-dimensional organization of the hippocampal formation: a review of anatomical data. *Neuroscience*, 31(3), 571–591.
- Andersen, P., Bliss, T. V., Lomo, T., Olsen, L. I., and Skrede, K. K. 1969. Lamellar organization of hippocampal excitatory pathways. *Acta Physiol Scand*, 76(1), 4A–5A.
- Andersen, P., Soleng, A. F., and Raastad, M. 2000. The hippocampal lamella hypothesis revisited. *Brain Res*, 886(1–2), 165–171.
- Bartos, M., Vida, I., Frotscher, M., Geiger, J. R., and Jonas, P. 2001. Rapid signaling at inhibitory synapses in a dentate gyrus interneuron network. *J Neurosci*, 21(8), 2687–98.
- Bartos, M., Vida, I., Frotscher, M., Meyer, A., Monyer, H., Geiger, J. P. R., and Jonas, P. 2002. Fast synaptic inhibition promotes synchronized gamma oscillations in hippocampal interneuron networks. *Proc Natl Acad Sci USA*, 99(20), 13222–13227.
- Bathellier, B., Carleton, A., and Gerstner, W. 2008. Gamma oscillations in a nonlinear regime: a minimal model approach using heterogeneous integrate-and-fire networks. *Neural Comp*, 20(12), 2973–3002.
- Börgers, C., and Kopell, N. 2003. Synchronization in networks of excitatory and inhibitory neurons with sparse, random connectivity. *Neural Comp*, 15(3), 509–539.

- Börgers, C., and Kopell, N. 2005. Effects of noisy drive on rhythms in networks of excitatory and inhibitory neurons. *Neural Comp*, 17(3), 557–608.
- Börgers, C., and Kopell, N. 2008. Gamma oscillations and stimulus selection. *Neural Comp*, 20, 383–414.
- Börgers, C., Epstein, S., and Kopell, N. 2005. Background gamma rhythmicity and attention in cortical local circuits: a computational study. *Proc Natl Acad Sci USA*, 102(19), 7002–7007.
- Börgers, C., Epstein, S., and Kopell, N. 2008. Gamma oscillations mediate stimulus competition and attentional selection in a cortical network model. *Proc Natl Acad Sci USA*, 105(46), 18023–8.
- Buhl, E. H., Cobb, S. R., Halasy, K., and Somogyi, P. 1995. Properties of unitary IPSPs evoked by anatomically identified basket cells in the rat hippocampus. *Eur J Neurosci*, 7(9), 1989–2004.
- Canolty, R. T., Edwards, E., Dalal, S. S., Soltani, M., Nagarajan, S. S., Kirsch, H. E., Berger, M. S., Barbaro, N. M., and Knight, R. T. 2006. High gamma power is phase-locked to theta oscillations in human neocortex. *Science*, 313, 1626–1628.
- Chapman, C. A., and Lacaille, J. C. 1999. Cholinergic induction of theta-frequency oscillations in hippocampal inhibitory interneurons and pacing of pyramidal cell firing. *J Neurosci*, 19, 8637–8645.
- Crook, S. M., Ermentrout, G. B., and Bower, J. M. 1998. Spike frequency adaptation affects the synchronization properties of networks of cortical oscillators. *Neural Comp*, 10(4), 837–854.
- Cunningham, M. O., Whittington, M. A., Bibbig, A., Roopun, A., LeBeau, F. E. N., Vogt, A., Monyer, H., Buhl, E. H., and Traub, R. D. 2004. A role for fast rhythmic bursting neurons in cortical gamma oscillations in vitro. *Proc Natl Acad Sci USA*, 101(18), 7152–7157.
- Dickson, C. T., Magistretti, J., Shalinsky, M. H., Fransen, E., Hasselmo, M. E., and Alonso, A. 2000. Properties and role of I(h) in the pacing of subthreshold oscillations in entorhinal cortex layer II neurons. *J Neurophysiol*, 83(5), 2562–2579.
- Diener, F. 1985a. Propriétés asymptotiques des fleuves. *C R Acad Sci Paris*, 302, 55–58.
- Diener, M. 1985b. Détermination et existence des fleuves en dimension 2. *C R Acad Sci Paris*, 301, 899–902.
- Dorval, A. D., Christini, D. J., and White, J. A. 2001. Real-time linux dynamic clamp: a fast and flexible way to construct virtual ion channels in living cells. *Ann Biomed Eng*, 29(10), 897–907.
- Dragoi, G., and Buzsáki, G. 2006. Temporal encoding of place sequences by hippocampal cell assemblies. *Neuron*, 50, 145–157.
- Dugladze, T., Vida, I., Tort, A. B., Gross, A., Otahal, J., Heinemann, U., Kopell, N. J., and Gloveli, T. 2007. Impaired hippocampal rhythmogenesis in a mouse model of mesial temporal lobe epilepsy. *Proc Natl Acad Sci USA*, 104(44), 17530–17535.
- Ermentrout, G. B. 1996. Type I membranes, phase resetting curves, and synchrony. *Neural Comp*, 8, 879–1001.
- Ermentrout, G. B., and Kopell, N. 1998. Fine structure of neural spiking and synchronization in the presence of conduction delay. *Proc Natl Acad Sci USA*, 95, 1259–1264.
- Ermentrout, B., Pascal, M., and Gutkin, B. 2001. The effects of spike frequency adaptation and negative feedback on the synchronization of neural oscillators. *Neural Comp*, 13, 1285–1310.
- Fisahn, A., Pike, F. G., Buhl, E. H., and Paulsen, O. 1998. Cholinergic induction of network oscillations at 40 Hz in the hippocampus in vitro. *Nature*, 394(6689), 186–189.
- Galán, R. F., Ermentrout, G. B., and Urban, N. N. 2005. Efficient estimation of phase-resetting curves in real neurons and its significance for neural-network modeling. *Phys Rev Lett*, 94(15), 158101.
- Gerstner, W., van Hemmen, J. L., and Cowen, J. 1996. What matters in neuronal locking? *Neural Comp*, 8, 1653–1676.
- Gillies, M. J., Traub, R. D., LeBeau, F. E. N., Davies, C. H., Gloveli, T., Buhl, E. H., and Whittington, M. A. 2002. A model of atropine-resistant theta oscillations in rat hippocampal area CA1. *J Physiol*, 543(Pt 3), 779–793.
- Gloveli, T., Dugladze, T., Saha, S., Monyer, H., Heinemann, U., Traub, R. D., Whittington, M. A., and Buhl, E. H. 2005a. Differential involvement of oriens/pyramidal interneurons in hippocampal network oscillations in vitro. *J Physiol*, 562(Pt 1), 131–147.

- Gloveli, T., Dugladze, T., Rotstein, H. G., Traub, R. D., Monyer, H., Heinemann, U., Whittington, M. A., and Kopell, N. J. 2005b. Orthogonal arrangement of rhythm-generating microcircuits in the hippocampus. *Proc Natl Acad Sci USA*, 102(37), 13295–13300.
- Goldin, M., Epszstein, J., Jorquera, I., Represa, A., Ben-Ari, Y., Crépel, V., and Cossart, R. 2007. Synaptic kainate receptors tune oriens-lacunosum moleculare interneurons to operate at theta frequency. *J Neurosci*, 27(36), 9560–9572.
- Golomb, D., and Hansel, D. 2000. The number of synaptic inputs and the synchrony of large sparse neuronal networks. *Neural Comp*, 12, 1095–1139.
- Gray, C. M. 1999. The temporal correlation hypothesis of visual feature integration: still alive and well. *Neuron*, 24(1), 31–47.
- Gutkin, B. S., Ermentrout, G. B., and Reyes, A. D. 2005. Phase-response curves give the responses of neurons to transient inputs. *J Neurophysiol*, 94, 1623–1635.
- Haas, J. S., and White, J. A. 2002. Frequency selectivity of layer II stellate cells in the medial entorhinal cortex. *J Neurophysiol*, 88(5), 2422–2429.
- Hamzei-Sichani, F., Kamasawa, N., Janssen, W. G. M., Yasumura, T., Davidson, K. G. V., Hof, P. R., Wearne, S. L., Stewart, M. G., Young, S. R., Whittington, M. A., Rash, J. E., and Traub, R. D. 2007. Gap junctions on hippocampal mossy fiber axons demonstrated by thin-section electron microscopy and freeze-fracture replica immunogold labeling. *Proc Natl Acad Sci USA*, 104(30), 12548–12553.
- Harris, K. D., Csicsvari, J., Hirase, H., Dragoi, G., and Buzsáki, G. 2003. Organization of cell assemblies in the hippocampus. *Nature*, 424(6948), 552–556.
- Hebb, D. O. 1949. *The Organization of Behavior: A Neuropsychological Theory*. New York: Wiley.
- Hines, M. L., and Carnevale, N. T. 1997. The NEURON simulation environment. *Neural Comp*, 9(6), 1179–1209.
- Hu, H., Vervaeke, K., and Storm, J. F. 2002. Two forms of electrical resonance at theta frequencies, generated by M-current, h-current and persistent Na⁺ current in rat hippocampal pyramidal cells. *J Physiol*, 545(Pt 3), 783–805.
- Itskov, V., Pastalkova, E., Mizuseki, K., Buzsáki, G., and Harris, K. D. 2008. Theta-mediated dynamics of spatial information in hippocampus. *J Neurosci*, 28, 5959–5964.
- Katona, I., Acsády, L., and Freund, T. F. 1999. Postsynaptic targets of somatostatin-immunoreactive interneurons in the rat hippocampus. *Neuroscience* 88(1), 37–55.
- Kay, L. M. 2003. Two species of gamma oscillations in the olfactory bulb: dependence on behavioral state and synaptic interactions. *J Integr Neurosci*, 2(1), 31–44.
- Klausberger, T., Magill, P. J., Márton, L. F., Roberts, J. D. B., Cobden, P. M., Buzsáki, G., and Somogyi, P. 2003. Brain-state- and cell-type-specific firing of hippocampal interneurons in vivo. *Nature*, 421, 844–848.
- Kopell, N., and Ermentrout, G. B. 2002. Mechanisms of phase-locking and frequency control in pairs of coupled neural oscillators. In *Handbook on Dynamical Systems: Toward Applications*. Ed. B. Fiedler, Vol. 2, Elsevier, Amsterdam, 3–54.
- Kopell, N., and Ermentrout, B. 2004. Chemical and electrical synapses perform complementary roles in the synchronization of interneuronal networks. *Proc Natl Acad Sci USA*, 101(43), 15482–15487.
- Kopell, N. 2005. Does it have to be this complicated? Focus on “Single-column thalamocortical network model exhibiting gamma oscillations, spindles, and epileptogenic bursts”. *J Neurophysiol*, 93(4), 1829–1830.
- Lawrence, J. J., Saraga, F., Churchill, J. F., Statland, J. M., Travis, K. E., Skinner, F. K., and McBain, C. J. 2006. Somatodendritic Kv7/KCNQ/M channels control interspike interval in hippocampal interneurons. *J Neurosci*, 26(47), 12325–12338.
- Lewis, T. J., and Rinzel, J. 2000. Self-organized synchronous oscillations in a network of excitable cells coupled by gap junctions. *Network Comput Neural Syst*, 11, 299–320.
- Lewis, T. J., and Rinzel, J. 2001. Topological target patterns and population oscillations in a network with random gap junctional coupling. *Neurocomputing*, 763–768.
- Middleton, S., Jalics, J., Kispersky, T., Lebeau, F. E. N., Roopun, A. K., Kopell, N. J., Whittington, M. A., and Cunningham, M. O. 2008. NMDA receptor-dependent switching

- between different gamma rhythm-generating microcircuits in entorhinal cortex. *Proc Natl Acad Sci USA*, 105(47), 18572–18577.
- Munro, E. C. 2008. The axonal plexus: a description of the behavior of a network of axons connected by gap junctions. Ph.D. thesis, Tufts University.
- Netoff, T. I., Acker, C. D., Bettencourt, J. C., and White, J. A. 2005a. Beyond two-cell networks: experimental measurement of neuronal responses to multiple synaptic inputs. *J Comput Neurosci*, 18(3), 287–295.
- Netoff, T. I., Banks, M. I., Dorval, A. D., Acker, C. D., Haas, J. S., Kopell, N., and White, J. A. 2005b. Synchronization in hybrid neuronal networks of the hippocampal formation. *J Neurophysiol*, 93(3), 1197–1208.
- Olufsen, M., Whittington, M., Camperi, M., and Kopell, N. 2003. New functions for the gamma rhythm: population tuning and preprocessing for the beta rhythm. *J Comput Neurosci*, 14, 33–54.
- Oprisan, S. A., Prinz, A. A., and Canavier, C. C. 2004. Phase resetting and phase locking in hybrid circuits of one model and one biological neuron. *Biophys J*, 87, 2283–2298.
- Orban, G., Kiss, T., and Erdi, P. 2006. Intrinsic and synaptic mechanisms determining the timing of neuron population activity during hippocampal theta oscillation. *J Neurophysiol*, 96(6), 2889–2904.
- Oren, I., Nissen, W., Kullmann, D. M., Somogyi, P., and Lamsa, K. P. 2009. Role of ionotropic glutamate receptors in long-term potentiation in rat hippocampal CA1 oriens-lacunosum moleculare interneurons. *J Neurosci*, 29(4), 939–950.
- Pastalkova, E., Itskov, V., Amarasingham, A., and Buzsáki, G. 2008. Internally generated cell assembly sequences in the rat hippocampus. *Science*, 321, 1322–1327.
- Pervouchine, D. D., Netoff, T. I., Rotstein, H. G., White, J. A., Cunningham, M. O., Whittington, M. A., and Kopell, N. J. 2006. Low-dimensional maps encoding dynamics in entorhinal cortex and hippocampus. *Neural Comp*, 18(11), 2617–2650.
- Reinker, S., Li, Y.-X., and Kuske, R. 2006. Noise-induced coherence and network oscillations in a reduced bursting model. *Bull Math Biol*, 68(6), 1401–1427.
- Rotstein, H. G., Pervouchine, D. D., Acker, C. D., Gillies, M. J., White, J. A., Buhl, E. H., Whittington, M. A., and Kopell, N. 2005. Slow and fast inhibition and an H-current interact to create a theta rhythm in a model of CA1 interneuron network. *J Neurophysiol*, 94(2), 1509–1518.
- Rotstein, H. G., Oppermann, T., White, J. A., and Kopell, N. 2006. The dynamic structure underlying subthreshold oscillatory activity and the onset of spikes in a model of medial entorhinal cortex stellate cells. *J Comput Neurosci*, 21(3), 271–292.
- Saraga, F., Wu, C. P., Zhang, L., and Skinner, F. K. 2003. Active dendrites and spike propagation in multi-compartment models of oriens-lacunosum/moleculare hippocampal interneurons. *J Physiol*, 552(3), 502–509.
- Senior, T. J., Huxter, J. R., Allen, K., O'Neill, J., and Csicsvari, J. 2008. Gamma oscillatory firing reveals distinct populations of pyramidal cells in the CA1 region of the hippocampus. *J Neurosci*, 28(9), 2274–2286.
- Serenevay, A. 2007. Dynamic mechanisms in networks of interneurons with periodic drives. Ph.D. thesis, Boston University.
- Sharp, A. A., O'Neil, M. B., Abbott, L. F., and Marder, E. 1993. Dynamic clamp: computer-generated conductances in real neurons. *J Neurophysiol*, 69(3), 992–995.
- Singer, W., and Gray, C. M. 1995. Visual feature integration and the temporal correlation hypothesis. *Annu Rev Neurosci*, 18, 555–586.
- Tort, A. B. L., Rotstein, H. G., Ducladze, T., Gloveli, T., and Kopell, N. J. 2007. On the formation of gamma-coherent cell assemblies by oriens lacunosum-moleculare interneurons in the hippocampus. *Proc Natl Acad Sci USA*, 104(33), 13490–13495.
- Tort, A. B. L., Kramer, M. A., Thorn, C., Gibson, D. J., Kubota, Y., Graybiel, A. M., and Kopell, N. 2008. Dynamic cross-frequency couplings of local field potential oscillations in rat striatum and hippocampus during performance of a T-maze task. *Proc Natl Acad Sci USA*, 105(51), 20517–20522.

- Traub, R. D., and Miles, R. 1991. *Neuronal Networks of the Hippocampus*. Cambridge, UK: Cambridge University Press.
- Traub, R. D., Jefferys, J. G. R., and Whittington, M. 1997. Simulation of gamma rhythms in networks of interneurons and pyramidal cells. *J Comput Neurosci*, 4, 141–150.
- Traub, R. D., Bibbig, A., Fisahn, A., LeBeau, F. E. N., Whittington, M. A., and Buhl, E. H. 2000. A model of gamma-frequency network oscillations induced in the rat CA3 region by carbachol in vitro. *Eur J Neurosci*, 12, 4093–4106.
- Traub, R. D., Kopell, N., Bibbig, A., Buhl, E. H., LeBeau, F. E. N., and Whittington, M. A. 2001. Gap junctions between interneuron dendrites can enhance long-range synchrony of gamma oscillations. *J Neurosci*, 21, 9478–9486.
- Traub, R. D., Bibbig, A., LeBeau, F. E. N., Buhl, E. H., and Whittington, M. A. 2004. Cellular mechanisms of neuronal population oscillations in the hippocampus in vitro. *Annu Rev Neurosci*, 27, 247–278.
- Traub, R. D., Contreras, D., Cunningham, M. O., Murray, H., LeBeau, F. E. N., Roopun, A., Bibbig, A., Wilent, W. B., Higley, M. J., and Whittington, M. A. 2005. Single-column thalamocortical network model exhibiting gamma oscillations, sleep spindles, and epileptogenic bursts. *J Neurophysiol*, 93(4), 2194–2232.
- Tukker, J., Fuentealba, P., Hartwich, K., Somogyi, P., and Klausberger, T. 2007. Cell type-specific tuning of hippocampal interneuron firing during gamma oscillations in vivo. *J Neurosci*, 27(31), 8184–8189.
- van Vreeswijk, C., Abbott, L. F., and Ermentrout, G. B. 1994. When inhibition not excitation synchronizes neural firing. *J Comput Neurosci*, 1, 313–322.
- Wang, X.-J., and Buzsáki, G. 1996. Gamma oscillation by synaptic inhibition in a hippocampal interneuronal network model. *J Neurosci*, 16, 6402–6413.
- White, J., Chow, C., Ritt, J., Soto-Trevino, C., and Kopell, N. 1998a. Synchronization and oscillatory dynamics in heterogeneous, mutually inhibited neurons. *J Comput Neurosci*, 5, 5–16.
- White, J. A., Klink, R., Alonso, A., and Kay, A. R. 1998b. Noise from voltage-gated ion channels may influence neuronal dynamics in the entorhinal cortex. *J Neurophysiol*, 80, 262–269.
- White, J. A., Banks, M. I., Pearce, R. A., and Kopell, N. J. 2000. Networks of interneurons with fast and slow gamma-aminobutyric acid type A (GABAA) kinetics provide substrate for mixed gammatheta rhythm. *Proc Natl Acad Sci USA*, 97(14), 8128–8133.
- Whittington, M. A., Jefferys, J. G., and Traub, R. D. 1996. Effects of intravenous anaesthetic agents on fast inhibitory oscillations in the rat hippocampus in vitro. *Br J Pharmacol*, 118(8), 1977–1986.
- Whittington, M. A., Traub, R. D., Kopell, N., Ermentrout, B., and Buhl, E. H. 2000. Inhibition-based rhythms: experimental and mathematical observations on network dynamics. *Int J Psychophysiol*, 38, 315–336.
- Wittner, L., Henze, D. A., Zaborszky, L., and Buzsáki, G. 2007. Three-dimensional reconstruction of the axon arbor of a CA3 pyramidal cell recorded and filled in vivo. *Brain Struct Funct*, 212(1), 75–83.
- Wulff, P., Ponomarenko, A. A., Bartos, M., Korotkova, T. M., Fuchs, E. C., Böhner, F., Both, M., Tort, A. B. L., Kopell, N., Wisden, W., and Monyer, H. 2009. Hippocampal theta rhythm and its coupling with gamma oscillations require fast inhibition onto parvalbumin-positive interneurons. *Proc Natl Acad Sci USA*, 106(9), 3561–3566.